The structure of sitting-atop complexes of metalloporphyrins studied by theoretical methods

Shen, Yong; Ryde, Ulf

Published in:
Journal of Inorganic Biochemistry

DOI:
10.1016/j.jinorgbio.2004.01.004

2004

Document Version:
Peer reviewed version (aka post-print)

The structure of sitting-atop complexes of metalloporphyrins studied by theoretical methods

Yong Shen[a,c] and Ulf Ryde[b]

[a] Department of Inorganic Chemistry

[b] Department of Theoretical Chemistry

Lund University

Chemical Centre

P. O. Box 124

S-221 00 Lund

Sweden

[c] Department of Chemistry

Zhongshan University

510275, Guangzhou

P. R. China

Correspondence to Ulf Ryde

E-mail: Ulf.Ryde@teokem.lu.se; Phone: +46 – 46 2224502; Fax: +46 – 46 2224543

2017-03-19

Abstract

The metallation of tetrapyrroles is believed to proceed via a sitting-atop (SAT) complex, in which some of the pyrrole nitrogen atoms are still protonated and the metal ion resides above the ring plane. No crystal structure of such a complex has been presented, but NMR and EXAFS (extended X-ray absorption fine structure) data has been reported for Cu^{2+} in acetonitrile. We have used density functional calculations to obtain reasonable models for SAT complexes of porphyrins with Mg^{2+}, Fe^{2+}, and Cu^{2+}. The results show that there are many possible SAT complexes with 1–5 solvent molecules, one or two metal ions, and cis or trans protonation of the porphyrin ring. Many of these have similar energies and their relative stabilities vary with the metal ion. A complex with two cis pyrrolenine nitrogens atoms and 2–4 solvent molecules coordinated to Cu^{2+} fits the NMR and EXAFS data best. However, we cannot fully exclude the possibility that what is observed is rather a mixture of a doubly protonated porphyrin and the copper porphyrin. Mg^{2+} has a lower affinity for porphyrin and stronger affinity for water, so a complex with five water molecules and only one bond to porphyrin seems to be most stable. For Fe^{2+}, a cis structure with two first-sphere water molecules and four interactions to the porphyrin seems to be most likely.

Keywords: sitting-atop complex, haem, chlorophyll, porphyrin distortion, ligand exchange, density functional theory.

Introduction

Metal complexes of tetrapyrroles are common in biological systems, with haem, chlorophyll, vitamin B_{12}, and coenzyme F430 as typical examples. They provide essential cofactors in a huge number of proteins and enzymes. Therefore, they have attracted much interest from all parts of chemistry [1]. One important and interesting step in the formation of these cofactors is the insertion of the metal ion. This step has been extensively studied both in solution [2-7] and in biological systems, where the reaction is catalysed by so-called chelatases [8-13].

The metallation of a porphyrin molecule in solution is believed to consist of the following steps [2-7]: deformation of the porphyrin ring, outer-sphere association of the solvated metal ion and the porphyrin, exchange of a solvent molecule with the first pyrrolenine nitrogen atom (i.e. a porphyrin nitrogen atom without any bound hydrogen), chelate-ring closure with the expulsion of more solvent molecules, first deprotonation of a pyrrole nitrogen atom, and second deprotonation of the other nitrogen atom, which will lead to the formation of the metalloporphyrin.

The intermediate formed after the chelate-ring closure is often called the *sitting-atop* (SAT) *complex* [14]. Thus, a SAT complex is a complex of a doubly protonated porphyrin ring with a metal ion, where the latter coordinates to both of the unprotonated pyrrole nitrogen atoms. The protons on two of the pyrrole nitrogen atoms prohibits the metal ion to reside in the centre of the porphyrin plane; instead, it will lie above the ring plane and form bonds to a number of solvent molecules. This complex has been much discussed. SAT complexes of porphyrins with Pt^{2+}, Cu^{2+}, and Rh^{+} have been reported [15-17] and kinetic evidence indicates that it exists for many other ions [18-21], but there is not yet any crystal structure of a SAT complex. However recently, SAT complexes of Cu^{2+} with various porphyrins in acetonitrile have been characterised by kinetic measurements, extended X-ray absorption fine structure (EXAFS) and nuclear magnetic resonance (NMR) methods [3,22,23]. The data was

interpreted as a six-coordinate complex with three kinds of Cu–N interactions with bond lengths of 205, 198, and 232 pm. It was suggested that these distances represent pyrrolenine nitrogen atoms of the porphyrin and acetonitrile nitrogen atoms at equatorial and axial sites, respectively [3]. Yet, other investigators have argued that no SAT complex is actually seen. Instead, they suggest that other species are observed, e.g. a doubly protonated porphyrin molecule [24-26].

Even if many theoretical investigations have been published for haem, chlorophyll, vitamin B_{12}, coenzyme F430, and even for ferrochelatase [e.g. 27-36] no quantum chemical studies seem to be available for SAT complexes. In this paper, we present quantum chemical structures of SAT complexes of porphyrins with Cu^{2+}, Mg^{2+}, and Fe^{2+}, with water or acetonitrile ligands. The results provide an interpretation of the experimental data and suggest the most stable SAT structures for the three metal ions. They also give information about the mechanism of metallation of porphyrins.

Methods

We have studied complexes of porphine ($PorH_2$, i.e. a porphyrin without any side chains), with two pyrrole rings protonated either in trans or cis. As metal ions we have used Mg^{2+} (the central ion in chlorophyll), Fe^{2+} (the central ion ion in haem), and Cu^{2+} (the metal ion used in the EXAFS and NMR experiments). The metal has been coordinated to 1–6 water or acetonitrile (AN, CH_3CN) molecules, and in many cases, solvent molecules have also been added to the second sphere of the metal ion (on the same side of the porphyrin ring as the metal ion, if not otherwise stated). Thus, we do not study only SAT complexes in the strict sense defined in the introduction, but all types of complexes of a doubly protonated porphyrin ring ($PorH_2$) with a solvated metal ion. We have used this wider definition because all our complexes are possible interpretations of the experimental data and they are probable intermediates in the metallation reaction.

Geometry optimisations were performed with the density functional BP86 method, which consists of Becke's 1988 gradient corrected exchange functional, combined with Perdew's 1986 correlation functional [37,38]. These calculations employed the 6-31G* basis set for all atoms, except for the metals, for which we used the TZVP basis (Mg) [39], or the DZP basis [40], enhanced with *p*, *d*, and *f*-type functions with exponents of 0.134915, 0.041843, 0.1244, and 1.339 (Fe, two *p* functions) and 0.174, 0.132, and 0.39 (Cu). These calculations were sped up (by a factor of ~5) by expansion of the Coulomb interactions in auxiliary basis sets, the resolution-of-identity approximation [41,42].

After the geometry optimisations, accurate energies were calculated using the three-parameter hybrid functional B3LYP, as implemented in the Turbomole package [43]. In these calculations, the 6-311+G(2d,2p) basis set was used for the light atoms (including Mg) and the basis set for Fe and Cu were enhanced with an *s* function (exponents Fe: 0.01377232 or Cu: 0.0155065; for Cu also with a *p* function with exponent 0.046199) and the single *f* function was replaced by two functions with exponents 2.5 and 0.8 (Fe) or 3.55 and 0.39 (Cu).

Such a two-stage procedure (a medium-sized basis set for geometry optimisations and a large basis set for energy calculations) has frequently been used before and has been shown to give accurate energies (energies are quite insensitive to the geometry on which they are calculated) [27,28,44]. It could perhaps be expected that diffuse functions are needed for geometry optimisations of the distorted porphyrins in this study. However, we have run several optimisations also with the 6-31+G* basis set (and the same basis set in the energy calculations), but this did not change the relative energies of the studied complexes by more than 1 kJ/mole.

In order to get a feeling of the effect of solvation on the relative energies of the various complexes, we have also calculated (single-point) solvation energies using the continuum conductor-like screening model (COSMO) [45], as implemented in Turbomole 5.5 **[46].** These calculations were performed with default values for all parameters (implying a water-like

probe molecule) and a dielectric constant (ε) of 80 for water complexes and 36.64 for acetonitrile (we used the same probe radius for water and acetonitrile to make the calculations more comparable and because the radius is poorly defined for an elongated molecule like acetonitrile). For the generation of the cavity, a set of atomic radii have to be defined. We used the optimised COSMO radii in Turbomole (130, 200, 183, and 172 pm for H, C, N, and O) [47]. For the metals, the same radius, 200 pm, was used. This radius of the metal has minor influence on the results, because the metals is hidden by the other ligands in all complexes.

The distortion (strain) energy of the porphyrin ring in the various complexes was estimated by removing all atoms except those in the porphyrin ring (i.e. $PorH_2$) and then calculating the single-point energy of it in this fixed geometry. This energy was the compared to that of $PorH_2$ in its optimum geometry, giving an estimate of how much the porphyrin ring is distorted in the various SAT complexes.

For a several complexes zero-point energy and thermal corrections to the Gibbs free energy (at 298 K and 1 atm pressure, using an ideal-gas approximation [48]) were calculated from a frequency calculation with the Gaussian98 software [49], using the same method and basis set as the geometry optimisation. The same software, method, and basis set was also used to calculate NMR isotropic shifts of some complexes, with the gauge-independent atomic orbital (GIAO) method [**50**].

All the other calculations were carried out with the Turbomole software, version 5.5 [51]. For Cu (doublet) and Fe (high-spin quintet state), unrestricted open-shell theory was employed. We made use of default convergence criteria, which imply self-consistency down to 10^{-6} Hartree (2.6 J/mole) for the energy and 10^{-3} a.u. for the maximum norm of the internal gradient. Several starting structures were tried for most complexes, but only the structure with the lowest energy of each type is reported.

Density functional methods, and in particular the BP86 method, have been shown to give excellent geometries for transition metal complexes, with errors in metal–ligand bond lengths of 0–5 pm [52]. Errors in the energy calculated with the B3LYP method with a large basis set

is in general less than 25 kJ/mole [27,28,53]. Calibrations on transition metal complexes have shown that the geometries and energies do not change significantly if the method or the basis sets are improved over the present level [54]. In order to check the performance of the current method on some relevant complexes, we optimised the structure of CuPor, $CuAn_6^{2+}$ and $CuAn_4^{+}$ and compared it to EXAFS and X-ray data. For CuPor, the optimised Cu–N bonds (202 pm) are identical to those measured by EXAFS [23], but 1–4 pm longer than distances obtained by X-ray crystallography on various porphyrins [55-58]. For $CuAn_6^{2+}$, the optimised Cu–N distances (4×200, 238, and 239 pm) are 1 pm longer (equatorial) or 1–2 pm shorter (axial) than those obtained by EXAFS methods [23]. For $CuAn_4^{+}$, our optimised Cu–N bonds (197 pm) are 2 pm shorter than distances observed in the crystal structure of $CuAn_4ClO_4$ [59]. Thus, our theoretical distances should be accurate to within 0–4 pm. If the complexes are reoptimised with constraints to the experimental bond lengths, the structures are destabilised (relative to the unconstrained structure) by less than 1 kJ/mole. This shows that systematic errors in the quantum chemical calculations do not significantly affect the energies of structures constrained to experimental data.

Result and Discussion

Sitting-atop complexes of Mg^{2+}

We started by optimising the structure of $Mg^{+2}PorH_2$ with a varying number of water molecules coordinated to magnesium, but giving the ion the opportunity to coordinate to the porphyrin nitrogen atoms. It turned out that a number of different complexes could be obtained with 1–5 water molecules in the first coordination sphere of the ion, as are shown in Figure 1 and Table 1.

In the complex with five water molecules (5+0 in Tables 1–2, and in Figure 1; “5+0” indicates that the complex has five first-sphere solvent molecules but no second-sphere solvent molecule), the magnesium ion forms one weak bond to a pyrrolenine nitrogen atom

(N_{Pyrn}; 230 pm; the bond length in MgPor, calculated by the same method is 207 pm) and five normal bonds to water molecules (206–214 pm; the bond length in $Mg(H_2O)_6$, calculated by the same method is 210 pm). Thus, this is not a true SAT complex, but rather the intermediate after the first ligand exchange reaction. The porphyrin is domed to improve the interaction between Mg^{2+} and N_{Pyrn}, and also the hydrogen bond between a water molecule and the other N_{Pyrn}. The distortion energy of the porphyrin ring, compared to the optimised (planar) vacuum structure is 36 kJ/mole. This is only 8 kJ/mole more than for the outer-sphere complex of $PorH_2$ and a Mg^{2+} ion coordinated to six water molecules (6+0).

In the corresponding complex with four water molecules (4+0), Mg^{2+} forms bonds to both the N_{Pyrn} atom (244 and 247 pm). Thus, it is a true SAT complex with the Mg^{2+} ion almost above the centre of the porphyrin ring. Therefore, the Mg–N_{Pyr} distances (i.e. to the protonated pyrrole nitrogen atoms) also become quite short (267 pm), and the porphyrin ring becomes saddled, which is also the case for all the other complexes with two Mg–N bonds. The Mg–O distances are all somewhat elongated: 223–224 pm. The distortion energy of the porphyrin molecule is appreciably larger than for the complex with five water molecules, 93 kJ/mole.

In the complex with three water molecules (3+0), the two Mg– N_{Pyrn} bonds become stronger and one of the Mg– N_{Pyr} distances becomes appreciably shorter. Therefore Mg remains approximately octahedrally six coordinate. When another water molecule is removed (2+0), the complex becomes almost symmetric with two short Mg– N_{Pyrn} bond and two longer Mg– N_{Pyr} bonds. Finally, if only one water molecule is kept (1+0), the Mg–N distances are shortened even more and the Mg–O bond becomes very short, reflecting that the coordination number has been reduced to five. As expected, the distortion energy of the porphyrin ring is largest in this complex, 195 kJ/mole.

In all these five complexes, we have kept the central protons on the porphyrin on the opposite (trans) nitrogen atoms. However, for some metals, it has been suggested that the SAT complex is instead formed when the protons reside on two cis nitrogen atoms [15]. For the

free $PorH_2$ molecule, this cis complex is destabilised by 32 kJ/mole (in water solution). Such cis structures can also be found for most complexes. For example, the complex with four water molecules (4+0 cis in Tables 1 and 2) has two rather strong Mg– N_{Pyrn} bonds and four mostly elongated Mg–O bonds. The distances to the two N_{Pyrn} atoms are long. The porphyrin ring is still saddled, but much more on the N_{Pyrn} side than on the other side. This leads to a distortion energy that is larger than for the corresponding trans structure.

Moreover, there is a series of complexes where Mg forms only one bond to the porphyrin, whereas the other N_{Pyrn} atom forms a hydrogen bond to a metal-bound water molecule. We call this type of complexes 1N in the Tables and Figures. With less than five water molecules, these complexes have a lowered coordination number of the Mg ion.

Consequently, there are 14 different complexes with 1–6 first-sphere water molecules, trans or cis coordination, and one or two bonds to N_{Pyrn} (there is no 5+0 complex that is not 1N and we could not obtain any 1+0 1N complex). All these complexes are probable intermediates in the metallation reaction and also possible candidates for the experimentally observed SAT complex. A way to judge the importance of the various complexes is to calculate their relative energies, as is in Table 2. Unfortunately, this comparison is far from trivial. Of course, only complexes with the same number of atoms can be compared. Therefore, only the trans, cis, and 1N complexes with the same number of water molecules can be directly compared. Such a comparison shows that the trans complexes are most stable with one and two water molecules, the cis complex with three water molecules, and the 1N complex with four and five water molecules.

In order to compare complexes with a different number of first-sphere water molecules, we have to optimise complexes with water molecules also in the second coordination sphere of the Mg ion, hydrogen bonded to the first-sphere waters (the geometry of these structures is included in the supplementary material). This is complicated by the fact that the number of local minima with different hydrogen-bond pattern rapidly increases, so it becomes hard to

find the most favourable structure. Moreover, it is hard to obtain any conclusive results with a restricted number of water molecules. For example, a series of complexes with the same number of water molecules (2–5), either all in the first sphere or with one in the second coordination sphere, indicate that the one with a second-sphere water molecule is always more stable by 19, 19, 6–50, and 24–30 kJ/mole, respectively (–1, 4, –7 to 43, and 11–20 kJ/mole in water solution).

Furthermore, the result of such an investigation depends on the number of water molecules. Thus, with a total of four water molecules, the 3+1 1N complex is most stable, whereas with six water molecules, the 4+2 1N complex is more stable. The reason for this is probably that too few water molecules are included. It is most likely that the apparent stability of the 1N complexes with a reduced coordination number (3+*n* 1N and 4+*n* 1N) are an artefact. Their stability merely reflects that hydrogen bonds to the first-sphere water molecules are more favourable than direct binding to the Mg ion as the fifth or sixth ligand. The reason for this is that the first-sphere water molecules are strongly polarised by the metal ion and therefore will form very strong hydrogen bonds. However, if additional water molecules were added, it would ultimately be more favourable for a water molecule to bind directly to the Mg ion, rather than to bind in the third or a higher coordination sphere (because the binding energy of the water molecule to the Mg ion is larger than the average hydrogen-bond strength in bulk water). This explains the lowered stability of the 3+*n* 1N complex when going from four to six molecules.

Thus, our best results should be those with six water molecules. Judging from these and ignoring the 4+2 1N and 3+3 1N complexes, we see that the most stable structures are the 6+0 and 5+1 1N complexes, the latter being most stable in vacuum, the former in water solution (by 21 kJ/mole, including thermodynamic effects). The 4+2 cis complex is the most stable true SAT complex (i.e. with two bonds between Mg and the N_{Pyrn} atoms), 20–40 kJ/mole less stable. Yet, only extensive calculations with a large number of water molecules can give a

conclusive answer to what structure is most stable.

Sitting-atop complexes of Cu^{2+} with water

We have seen that we can obtain reasonable sitting-atop structures of porphine and Mg. However, they differ quite extensively from the structure suggested for the SAT complex based on the EXAFS data, which was been interpreted as a six-coordinate site with Cu–N bonds of 205, 198, and 232 pm to N_{Pyrn} and to N_{AN} at equatorial and axial sites, respectively [3]; the corresponding Mg^{2+} complex with four water molecules had much longer Mg–N_{Pyrn} bonds (243–246 pm or 223 pm in the cis complex). Therefore, we have also studied SAT complexes of Cu^{2+}. We started to study water complexes so that we can directly compare with the results obtained with Mg^{2+}. The results are collected in in Figure 2 and in Tables 3 and 4.

The behaviour of Cu^{2+} is quite different from that of Mg^{2+}. The reason for this is mainly that Cu^{2+} is much softer than Mg^{2+} [60]. Therefore, copper has a stronger affinity for the pyrrole nitrogen atoms, but a lower affinity for water. In these cluster calculations, this means that we never find any six-coordinate copper complexes. Instead, copper prefers to be four-coordinate and additional water molecules end up in the second-sphere (i.e. it is more favourable to form hydrogen bonds to the other water molecules than to bind directly to copper). For example, our most stable structure of $Cu(H_2O)_6$ has only four first-sphere water molecules. This is partly an effect of the Jahn–Teller instability of Cu^{2+}, leading to square-planar structures, possibly with one or two week axial ligands [60]. Of course, it is also an effect of the low number of water molecules included in the calculations. If more solvent molecules were included in the calculations, five- or six-coordinate complexes would probably also be obtained. However, it clearly reflects a reduced affinity of copper to water. This is confirmed by recent experimental and theoretical data, which indicate that Cu^{2+} actually is mainly five-coordinate in water solution [61].

Finally, Cu^{2+} also has the possibly to be reduced to Cu^{+}, and for the SAT complexes the Cu^{+}–

$PorH_2^{\bullet}$ radical state is close in energy to the Cu^{2+}–$PorH_2$ state, and they can often both be found for the same complex (but with different geometries). Therefore, we have included the spin density on the copper ion for all complexes in Table 3. A population of 0.45-0.62 *e* is indicative of Cu(II), whereas Cu(I) has a lower population (typically ~0.25 *e*). Some complexes have intermediate spin density. The Cu(I) complexes are also characterised by high spin densities on the porphyrin carbon atoms, whereas the Cu(II) states have the remaining spin located mainly on the four equatorial ligands (N or O). The result of these differences is that many of the Mg SAT complexes were not found for Cu^{2+} (those with a high coordination number), whereas several new complexes were found for Cu^{2+}.

Cu^{2+} SAT complexes were found with 1–4 first-sphere water molecules. However, those with three and four first-sphere water molecules were quite hard to find and easily reorganised to other complexes. The complex with four first-sphere water molecules (4+0 1N) is approximately trigonal bipyramidal with one Cu–N_{Pyrn} bond (206 pm; the corresponding bond in CuPor is 202 pm) and four rather weak bonds to water (202–230 pm, compared to 196–200 pm for $Cu(H_2O)_4$). The spin population on Cu is 0.44 *e,* so it is clearly Cu(II). The porphyrin ring is only slightly saddled. One of the water molecules forms a hydrogen bond to the other N_{Pyrn} atom, so it is of the 1N type. No complex with two bonds to the porphyrin could be found.

The complex with three first-sphere water molecules is also of the 1N type (3+0 1N). It is almost square planar with one Cu–N_{Pyrn} bond and three Cu–O bonds. It has a quite low spin population on Cu (0.39 *e*), but we have also obtained another complex with an even lower Cu population (0.32 *e*) and higher populations on the methine links, and an almost tetrahedral structure (3+0 1N Cu^{I}). It is 4 kJ/mole more stable (6 kJ/mole less stable in water).

With two first-sphere water molecules, we obtained the first true SAT complex (2+0). It is quite similar to the Mg complex with two Cu–N_{Pyrn} bonds of 225 pm, two weak Cu–N_{Pyr} interactions at 247–261 pm, and two Cu–O bonds of 209 pm. The porphyrin is strongly

saddled with a distortion energy of 99 kJ/mole. It is clearly Cu(II).

However, there is also a Cu(I) complex with two first-sphere water molecules (2+0 Cu^{I}). It is similar to the Cu(II) complex, but with the O–Cu–O plane rotated 90° with respect to the porphyrin ring. Thereby, the copper ion coordination becomes tetrahedral. It has shorter Cu–N_{Pyrn} bonds but longer Cu–N_{Pyr} and Cu–O bonds. It is 9 kJ/mole more stable than the Cu(II) complex in water.

An even more stable complex can be found if the cis isomer of $PorH_2$ is used (2+0 cis). In this complex, Cu forms a square-planar structure with two strong Cu–N_{Pyrn} bonds of 198–199 pm and two rather strong Cu–O bonds of 203–206 pm. The Cu–N_{Pyr} distances are ~310 pm. The distortion of the porphyrin ring is unsymmetric but larger than for the two trans complexes, 123 kJ/mole. It is clearly Cu(II) and it is 65 kJ/mole more stable than the Cu(I) form.

However, a similar structure can also be obtained with trans $PorH_2$ (2+0 altcis). In this, Cu forms bonds to one N_{Pyrn} (195 pm), one N_{Pyr} (224 pm), and to two waters. The water with the longer bond also forms a hydrogen bond to the other N_{Pyrn}. Yet, this complex is 42 kJ/mole less stable than the other cis complex. The strain energy is intermediate between the 1N and 2N structures, 89 kJ/mole.

We have also obtained a normal 1N complex with two first-sphere water molecules (2+0 1N). It is trigonal three-coordinate, with a strong Cu–N_{Pyrn} bond and two strong Cu–O bonds. As usual, one water molecule forms a hydrogen bond to the other N_{Pyrn} atom. It is a Cu(I) complex and 29 kJ/mole in water less stable than the cis complex.

Finally, we have also found two complexes with only one first-sphere water molecule, similar to the corresponding Mg^{2+} complexes, a trans complex and a 10 kJ/mole less stable cis complex.

It has been suggested that SAT complexes can also be found with two metal ions, one on each side of the porphyrin ring [62]. For Mg^{2+}, no such structure could not be found (one of

the ions always dissociated), but for Cu^{2+}, it exists. The complex is essentially a dimer of the 1N structure with three waters: Each copper ion is four-coordinate with a rather weak Cu–N_{Pyrn} bond (207–212 pm) and three Cu–O bonds. The porphyrin strain energy is approximately twice as large as that of the 3+0 1N complex, 65 kJ/mole. In fact, we have found two such complexes, one with an almost tetrahedral coordination and one almost square planar. The former is 23 kJ/mole less stable in water. If additional water molecules are added to these structures, they end up in the second coordination sphere.

Among the complexes with two water molecules, that with one first-sphere water (1+1) is most stable in vacuum (12 kJ/mole more stable than the 2+0 cis complex), whereas in water solution, the 2+0 cis complex is 10 kJ/mole more stable. Zero-point, entropy, and thermal effects have little influence (less than 1 kJ/mole) on these energies. With three water molecules, the 2+1 cis complex is most stable, followed by the 2+1 1N (2–4 kJ/mole less stable) and the 1+2 complexes (16–26 kJ/mole less stable), both in vacuum and in water. The same applies with four water molecules, but there the 3+1 1N complex is also a candidate, 9–12 kJ/mole less stable than the 2+2 cis complex. Finally, the complex with two copper ions is also a candidate of the most stable SAT complex with Cu^{2+}, but the 2+0 cis complex plus a $Cu(H_2O)_4$ cluster is 102 kJ/mole more stable than the two-copper complex in water solution. Thus, the results indicate that the cis complex with two first-sphere water molecules is the most stable SAT complex with Cu^{2+} and water.

Sitting-atop complexes of Cu^{2+} with acetonitrile

Next, we studied SAT complexes of Cu^{2+} with acetonitrile, with the aim of comparing with the experimental EXAFS and NMR data. Even if we saw that the four -coordinate cis complex seemed to be most stable among the water complexes with Cu^{2+}, we cannot assume that this is also the case for AN, because the two solvents are quite different. In particular, AN has no polar hydrogen atoms, so second-sphere AN molecules can only form weak

interactions with CH groups. Therefore, we did also a complete investigation of possible SAT of Cu^{2+} and AN.

As can be seen in Tables 5 and 6, we find the same complexes for AN as for water (except for the complex with four first-sphere AN molecules, the Cu(II) complex with two first-sphere AN molecules, and the altcis complex). The main difference is that the 1N complexes seem to be more stable for AN than for water. Thus, the 2+0 1N complex is the most stable complex with two AN molecules in vacuum (5 kJ/mole more stable than the cis complex, but 14 kJ/mole *less* stable in AN solution). Likewise, the 3+0 1N complex is the most stable complex with three AN molecules in vacuum (the 2+1 cis complex is 18 kJ/mole less stable, but 7 kJ/mole more stable in solution). With four AN molecules, the 3+1 1N complex is most stable by both in vacuum and solution 23–33 kJ/mole. Therefore, the 1N complexes have to been taken into consideration also.

As mentioned above, the EXAFS results were interpreted as a six-coordinate trans complex with three kinds of Cu–N interactions, each with approximately two nitrogen atoms and bond lengths of 205, 198, and 232 pm for N_{Pyrn} and for N_{AN} at equatorial and axial sites, respectively [3]. We have optimised such a structure, using constraints to the six EXAFS distances. The resulting structure is quite strange, as can be seen in Figure 3a (4+0): The porphyrin ring is sharply bent with a high strain energy (168 kJ/mole). This unusual deformation is caused by the close contacts between the axial AN molecules and the porphyrin ring. This repulsion increases the Cu–N_{Pyr} distances to 310 pm (they are 283 pm in the 2+0 complex). Most importantly, it is much less stable than other complexes with four AN molecules, by up to 217 kJ/mole in vacuum and 189 kJ/mole in solution. These energies are so large that it is highly unlikely that this is the best interpretation of the EXAFS data. Therefore, we will look for a better suggestion by comparing the optimised Cu–ligand distances with the EXAFS data.

The complex with one AN molecule (1+0) has a too long Cu–N_{AN} bond (210 pm) and too

short Cu–N_{Pyr} bonds (220 pm) compared to the experimental data. However, a complex with the five distances constrained to the experimental data (the Cu–N_{Pyrn} bonds to 205 pm, the Cu–N_{AN} bond to 198 pm, and the Cu–N_{Pyr} bonds to 232 pm) is only 7 kJ/mole less stable than the optimised complex. The structure is only slightly improved if it is optimised in a continuum solvent with the same dielectric constant as AN (the Cu–N_{AN} bond is still 209 pm), or if additional AN molecules are added around the complex, both on the same side as copper ion or on the opposite side (the Cu–N_{Pyr} bonds are still ~220 pm).

Likewise, the 1N complex with two first-sphere AN molecules (2+0 1N) is far from the experimental data (the Cu–N_{Pyrn} bond is too short, 197 pm). The 2+0 Cu(I) and the 3+0 cis complexes also fit the EXAFS data poorly (too long Cu–N_{Pyrn} bond or too Cu–N_{An} bonds, respectively).

The same applies to the complexes with two copper ions. The complex with two three-coordinate copper ions (2(Cu 2+0) 1N) has only three strong bonds, which all are too short (200–203 pm to N_{Pyrn} and 192–195 to AN). The four-coordinate complex (2(Cu 3+0) 1N) has reasonable bond lengths to AN (198–201 pm) but a too long bond to N_{Pyrn} (214 pm).

However, the four-coordinate 1N complex (3+0 1N) has quite reasonable Cu–N distances: 208 pm for the single Cu–N_{Pyrn} bond and 198–200 pm for the three first-sphere AN molecules. This fits the EXAFS data within 3 pm, but with the modification that there is only one interaction at 205 pm and three at 198 pm. If the structure is optimised in an acetonitrile-like solvent, the structure becomes even closer to the EXAFS structure, with a Cu–N_{Pyrn} bond of 207 pm and Cu–N_{AN} bonds of 198–199 pm. A complex with constraints to the EXAFS data (one bond to N_{Pyrn} and three bonds to AN) is only 0.4 kJ/mole less stable. Yet, a complex with two additional axial AN molecules, also constrained to the EXAFS data, is 79 kJ/mole less stable than the corresponding unconstrained complex. A complex with only one extra AN molecule is 32 kJ/mole less stable than the corresponding unconstrained complex in AN solution.

Finally, the cis complex with two first-sphere AN molecules (2+0 cis) is also a possible candidate. It has two Cu–N_{Pyrn} bonds of 201–204, and two Cu–N_{AN} bonds of 199–200 pm. When optimised in AN, the bonds contract and become more symmetric, so that the Cu–N_{AN} bonds become equal to the experimental ones, whereas the Cu–N_{Pyrn} bonds become 3 pm too short. If the bonds are constrained to the EXAFS data (205 and 198 pm), the complex is destabilised by 0.4 kJ/mole. The corresponding five-coordinate complex (3+0 cis) is also stable, but it is slightly less similar to the EXAFS results: The two Cu–N_{Pyrn} bonds are 2 pm too long, the two equatorial Cu–N_{AN} bonds are 5–6 pm too long, whereas the axial Cu–N_{AN} bond is 9 pm too short. However, if it is constrained to the experimental data, it is destabilised by only 1–2 kJ/mole in both vacuum and acetonitrile. If another axial AN molecules is added and constrained to 232 pm, the resulting complex is 74 kJ/mole less stable than an unconstrained complex in AN solution.

Finally, we should also consider the possibility that a SAT complex is actually not observed. In particular, Tsai et al. have suggested that what is observed in the experiments is rather a mixture of copper porphyrin and a doubly protonated (doubly cationic) porphyrin [24]. It this is true, then what is observed in the EXAFS experiment should be the copper porphyrin and possibly copper ions in AN solution. These complexes would give distances of 202 pm and 199 pm (equatorial) and 240 pm (axial), respectively, according to EXAFS data [23]. In out calculations, they are 202, 200, and 238–239 pm, respectively, as already mentioned. In Table 5, we can also see that $CuAN_5$ has distances of 197 and 204 pm (trigonal bipyramidal) or 199 and 214 pm (square pyramidal; the two structures are degenerate within 1 kJ/mole in vacuum). Thus, these results are reasonably close to the observed EXAFS bond lengths (differences of 3, 1, and 6 pm), with the change that there should be twice as many scatters at 198 pm than at 232 pm. However, the SAT complexes fit the data better.

Experimental NMR data have also been obtained for the putative SAT in AN [22]. It shows one peak for the H–N atoms, shifted by +0.8 ppm compared to the free porphyrin, and two

peaks for the β pyrrole hydrogen atoms, one singlet and one doublet. The former is said to correspond to pyrrolenine group coordinated to Cu and it is shifted by –0.1 ppm relative to the free porphyrin, whereas the doublet should arise from the pyrrole ring (with a NH group) and it is shifted by –0.2 ppm.

We have calculated the NMR spectra for the trans, cis, and 1N complexes with 2–4 (3–5 for the 1N complex) AN molecules and compared the isotropic NMR shifts of the H–N and β pyrrole atoms with those in $PorH_2$. For the β pyrrole atoms on $PorH_2$, the average of those on the pyrrole and pyrrolenine rings was taken (they differ by 0.2 ppm), because the protonation shifts rapidly on the NMR time scale (the experiment shows only one peak). The results are collected in Table 7.

Interestingly, the results for the 3+0 1N and 4+0 1N models, were widely different from those of the other models, with a negative shift of 23–32 ppm of the HN atoms, compared to more reasonable shifts of –1 to +2 ppm for the other seven models. These large shifts seems to come from a large spin density in the porphyrin ring: these two complexes are the only ones with a low spin density on copper (0.1–0.3; and therefore much spin in the porphyrin ring), whereas those with a large spin population on copper (~0.6) give the more reasonable shifts. If the copper ion is replaced by a Zn^{20} ion in these two complexes, the shifts on the HN atoms become +0.7–0.9. These two complexes will not be further discussed.

Among the remaining models, two give a negative shift for the HN atoms (the trans 4+0 complex and the 5+0 1N complex) in variance to the experimentally observed positive (0.8 ppm) shift. All the models have the correct negative shift of the β pyrrole atoms, but in the trans complexes, the (absolute) shift is larger for the atoms on the pyrrolenine ring that binds to Cu than on the pyrrole rings, in contrast to the experimental trend. Moreover, there are three different types of β atoms in the 1N complexes, pyrrole, and pyrrolenine with the nitrogen atom coordinated either to copper or hydrogen bonded to water. In the calculations, the shifts of these three types differ by 0.1–0.3 ppm and should therefore be experimentally

discerned.

On the other hand, the three cis models give qualitatively correct results, with a positive shift of the HN atoms and negative shifts of the β atoms atoms with the correct trend between the pyrrole and pyrrolenine atoms. However, all the shifts are appreciably larger than those observed experimentally, although the difference decreases to <0.7 ppm for the 4+0 cis complex. This overestimation applies to all the nine complexes, as does the reduction of the shifts when more AN. It may be an vacuum effect, but unfortunately it is not possible to calculate NMR shifts in solution with the available software.

Finally, we have also included the $PorH_4^{2+}$ and CuPor complexes in the investigation, because, Tsai and coworkers have suggested that these complexes, rather than a SAT complex, are actually observed in the NMR experiments [24]. In our calculations, CuPor showed a negative shift of –0.8 ppm, whereas the doubly protonated porphyrin showed a positive shift of 3.4 ppm for the HN atoms and a negative shift of –1.5 ppm for the β pyrrole atoms. Thus, these results also show the correct trends, but overestimate the experimental results by an amount similar to that of the 2+0 cis complex (but slightly more than the 4+0 cis complex). Thus, the accuracy of the present NMR calculations (1–2 ppm) is not enough to give an unambiguous interpretation of the experimental NMR results [63].

In conclusion, we see that we have two strong candidates for the SAT complex observed in the EXAFS experiment, the cis complex and the 1N complex. The 3+0 1N complex gives slightly better distances, but it has only one 205-pm interaction and three 198-pm interactions, contrary to the interpretation of two interactions of each type. The stability calculations indicate that the two complexes are almost equally stable. However, the cis complex fits the NMR results appreciably better than the 1N complex. Therefore, we believe that it is the best candidate for the observed SAT complex. It is likely that it in AN solution acquires additional axial ligand, but considering the destabilisation energies of such complexes and the fact that Cu^{2+} in water solution is dominantly five-coordinate [61], we think that there is mostly only

one axial ligand in the SAT complex (3+0 cis). Unfortunately, we cannot exclude the possibility that a SAT complex is actually not observed in the experiment, as Tsai and coworkers have suggested [24], although their suggested products fit both the EXAFS and NMR results slightly worse than does the cis SAT complex.

Sitting-atop complexes of Fe^{2+}

Finally, we have studied also complexes of $PorH_2$ and Fe^{2+}, the substrates in haem synthesis. As could be expected, the chemical properties of Fe^{2+} is intermediate between Mg^{2+} and Cu^{2+}. Thus, it prefers a coordination number of six (octahedral), but both four- (tetrahedral) and five-coordinate complexes are also found. Moreover, it has a quite strong affinity to both water molecules and the pyrrole nitrogen atoms. Therefore, we could obtain the same complexes as for Mg^{2+} and also some of the additional complexes found for Cu^{2+} (e.g. complexes with two iron ions). However, Fe^{2+} shows no tendency to be reduced. Instead, all the complexes are pure high-spin Fe^{2+}, with a spin population on Fe of 3.63–3.82 *e*.

The structures of all optimised Fe SAT complexes are shown in Figure 4 and the Fe–ligand distances are collected in Table 8. The relative energies of the complexes and the porphyrin strain energies are shown in Table 9. As with Mg, complexes with 1–6 first-sphere water molecules were obtained. Moreover, we found also cis and 1N variants of most complexes. Compared to Mg, the Fe–N_{Pyrn} distances are 5–11 pm shorter and the Fe–O bonds are 2–11 pm longer. However, the Cu complexes have even shorter bonds to N_{Pyrn} (by 2–6 pm) and longer water bonds (by 5–10 pm). A peculiarity with Fe is that in the 1N complexes, the water molecule hydrogen bonded to N_{Pyrn}, donates its proton to N_{Pyrn}, forming a deprotonated iron-bound hydroxide ion and $PorH_3^+$.

As for the Mg complexes, it is quite hard to decide which is the most stable SAT complex with Fe^{2+} and water. Judging from a series of complexes with six water molecules, the 4+2 1N complex is most stable, both in vacuum and in solution. However, it is essentially octahedral

with one open coordination site. Therefore, as was discussed above, it will probably reorganise to the 1N complex with five first-sphere water molecules if more waters are added. That 5+1 1N complex is ~22 kJ/mole less stable than the 4+2 1N complex. However, the cis complex with two first-sphere water molecules is more stable, only 5 kJ/mole less stable than the 4+2 1N complex (19 kJ/mole in water). This is probably the best candidate for a SAT complex of Fe^{2+}, but the trans 2+4 complex is only ~10 kJ/mole less stable.

The porphyrin strain energies are similar to those of the other metals: In general, Fe has a slightly larger stain energy than Mg, but lower than for Cu (for some of the complexes with few water ligands, the trend is different). This reflects the binding energy of the metal; it is lowest for the Mg complexes, intermediate for the Fe complexes, and highest for the Cu complexes (and higher for AN than for water), as can be seen in Table 10. In solution the trend remains, except that AN and water gives similar values, that with water normally being slightly higher.

The binding energy of the metal ion increases steadily with the number of water molecules (because the reference state was all the molecules separated). The binding energies of the SAT complexes are always much lower (~300 kJ/mole) than that the binding energy of the same metal in the porphyrin (MPor). However, it is similar to that of the metal ion coordinated to six solvent molecules. For Fe^{2+} and Cu^{2+}, the complexes with four or five solvent molecules have a binding energy (in solution) similar to that of $M(H_2O)_6$. However, for Mg^{2+}, the metal binding energy of $Mg(H_2O)_6$ is 62 kJ/mole lower than that of the 5+0 1N complex. Thus, there is an appreciable barrier against the chelatation reaction in solution that is not released until the porphyrin is deprotonated. This is probably the reason why the metallation of porphyrins with Mg^{2+} is several orders of magnitude slower than that of other metal ions [64] and why magnesium chelatase requires ATP hydrolysis, whereas ferrochelatase does not [8-13]. Counter-poise corrections to the basis-set superposition error is quite small, lowering the binding energy by 12–14 kJ/mole.

Conclusions

Using density functional calculations, we have studied various possible structures of SAT complexes between porphine and Mg^{2+}, Fe^{2+}, and Cu^{2+}, both in water and acetonitrile. We have seen that there are many possible candidates with similar energies. Therefore, and also for other reasons (we study complexes with only up to six water molecules and there are a large number of alternative configurations of each complex, especially of those with many second-sphere solvent molecules), it is hard to settle which structure is most stable.

For Cu^{2+} in AN, we can compare the results with experimental data. We have seen that a cis complex with two bonds to the porphyrin and two strongly bound solvent molecules fits the experimental data best. Moreover, it can be concluded that the experimental distances are very reasonable. However, it cannot be fully excluded that what is observed is rather a mixture of copper porphyrin and a doubly protonated porphyrin molecule [24].

The cis complex with two water molecules seems also to the most stable SAT complex for Cu^{2+} with water. The same is true also for Fe^{2+} in water, but there another candidate is a six-coordinate complex with five solvent molecules and only one bond to N_{Pyrn}.

Mg^{2+} differs from the other metals with a stronger affinity for water and a lower affinity for the porphyrin. Therefore, it seems to prefer the complex with only one bond to the porphyrin. It also has a lower binding energy in all complexes. Thus, we see that the various metals have different preferences and therefore also different structures of the SAT complex. Consequently, it is not enough to obtain experimental data for a SAT complex with one metal, but for all metals of interest.

The deformation energy of the porphyrin ring varies between 27 and 241 kJ/mole. It is highest for Cu^{2+} and lowest for Mg^{2+}, reflecting the strength of the various complexes, but the difference is not very large. Instead, the main difference in the deformation comes from the number of bonds between the metal and the porphyrin ring. Thus, the strain is a compromise

between the improvement of the metal–N_{Pyrn} interaction and the deformation of the ring system (some of the energy gained from the formation of the bonds between the metal and the porphyrin is used to deform the ring, but neither the metal–ligand bonds nor the ring structure is ideal). This shows that the deformation is coupled to bond formation and should probably not be considered as a separate step in the metallation reaction. In fact, an isolated porphyrin in water solution is also deformed, owing to improved hydrogen bonds between N_{Pyr} and N_{Pyrn} and the water molecules. The optimum structures of $PorH_2$ with two and four water molecules are shown in Fig. 6. They have porphyrin strain energies of 70–75 kJ/mole, i.e. more than many of the studied metal complexes. However, it should be noted that if a water molecule is added to the SAT complexes on the side opposite to the metal ion, the strain energy increases also for these complexes, e.g. to 87 kJ/mole for the Mg 5+1 1N complex (35 kJ/mole without the water molecule).

Already deformed porphyrins (e.g. N-alkylated porphyrins), which are known to be metallated at an increased rate [65], gains their increased rates because the porphyrin has a lower deformation energy both in the SAT intermediates and in the transition states. For example, the cis $[PorHCH_3Fe(H_2O)_2]^{2+}$ complex (Figure 5) has a deformation energy that is 34 kJ/mole, lower than for the corresponding complex with $PorH_2$ (45 kJ/mole for the trans complex). If the same energy difference applies in the transition state, this corresponds to a increase in the reaction rate of almost 6 orders of magnitude.

Finally, it is notable that there exists intermediates with any number of solvent molecules from six to one (at least for Mg and Fe). This indicates that the reaction mechanism is more complicated than normally assumed [3-7]. Thus, starting from six solvent molecules, the mechanism should involve all ligand-exchange steps (solvent to porphyrin) from six to one solvent molecules, via five, four, three and two first-sphere solvent molecules. We currently study the energetics of these reactions with quantum chemical methods.

It should be noted that the present calculations have been performed on a porphyrin model

without any side chains. It is known experimentally that both the kinetics and the geometry of the SAT complex is affected by the side chains of the porphyrin [3]. We have done some test calculations with tetraphenylporphyrin and octaethylporphyrin, which confirm the experimental findings that both the geometries (metal–ligand distances by up to 6 pm) and the relative energies change (by up to 13 kJ/mole) with these models. Thus, it must be recognised that the details of the present results may change with the actual side chains of the porphyrin. However, the energies involved are not larger than the inherent uncertainty of the present method (~25 kJ/mole) so the general conclusion should not be affected.

In conclusion, we have seen how we can gain valuable information about the porphyrin metallation mechanism and the structures of the intermediate with a combination of quantum chemical calculations and experimental data.

Acknowledgements

This investigation has been supported by grants from the Swedish research council, by computer resources of Lunarc at Lund University, and by a scholarship to Y. S. from Lund University.

References

1. L.R. Milgrom (1997) "The colours of life", Oxford University Press.
2. D.K. Lavallee, Coord. Chem. Rev. 61 (1985) 55-96.
3. M. Inamo, N. Kamiya, Y. Inada, M. Nomura, S. Funahashi Inorg. Chem. 40 (2001) 5636-5644.
4. P. Hambright in K. Smith, (Ed.) Dynamic coordination chemistry of metalloporphyrins, Elsevier, Amsterdam, 1975, pp. 233-278.
5. P. Hambright, J. Am. Chem. Soc. 96 (1974) 3123-3131.
6. D.K. Lavallee in J.F.Liebmann, A. Greenberg, (Eds.) Molecular structure and energetics, vol. 9: Mechanistic Principles of Enzymatic Activity, VCH, New York, 1988, pp. 279-314.
7. S. Funahashi, Inada, Y. Inamo, M. Analyt. Sci. 17 (2001) 917-927.
8. C.J. Walker, Willows RD Biochem J 327: (1997) 321–333
9. H.L. Shubert, Raux E, Wilson KS, Warren MJ Biochemistry 38: (1999) 10660–10669
10. E. Raux, H.L. Schubert, M.J. Warren, Cell Mol Life Sci 57: (2000) 1880–1893
11. C.-K. Wu, H.A. Dailey, J.P. Rose, A. Burden, V.M. Sellers, B.-C. Wang, Nature Str. Biol. 8: (2001) 156–160
12. S. Al-Karadaghi, M. Hansson, S. Nikonov, B. Jonsson, L. Hederstedt, Structure 5 (1997) 1501–1510
13. H.L. Schubert, E. Raux, A.A. Brindley, H.K. Leech, K.S. Wilson, C.P. Hill, M.J. Warren, EMBO J 21 (2002) 2068–2075
14. E.B. Fleischer, J.H. Wang, J. Am. Chem. Soc. 82 (1960) 3498.
15. J.P. Marcqet, T. Theophahanides, Can. J. Chem. 51 (1973) 219.
16. K. Letts, R.A. Mackay, Inorg. Chem. 14 (1975) 2993.
17. E.B. Fleischer, F. Dixon, Bioinorg. Chem. 7 (1977) 129.
18. T.P.G. Sutter, P. Hambright, Inorg. Chem. 31 (1992) 5089-5093.

19. Y. Inada, Y. Sugimoto, Y.Nakano, S. Funahashi, Chem. Lett. (1996) 881-882.

20. J. Takeda, T. Ohya, M. Sato, Inorg. Chem. 31 (1992) 2877-2880.

21. S. Funahashi, Y. Yamaguchi, M. Tanka, Bull. Chem. Soc. Jpn, 57 (1984) 204-208.

22. Y. Inada, Y. Sugimoto, Y. Nakano, Y. Itoh, S. Funahashi, Inorg. Chem. 37 (1998) 5519-5526.

23. Y. Inada, Y. Nakano, M. Inamo, M. Nomura, S. Funahashi Inorg. Chem. 39,(2001) 4793-4801.

24. C.-H. Tsai, J.-Y. Tung, J.-H. Chen, F.-L. Liao, S.-L.Wang, S.-S.Wang, L.-P. Hwang, C.-B. Chen, Polyhedron, 19 (2000) 633-639.

25. H. Baker, P. Hambright, L. Wagner, J. Am. Chem. Soc. 98 (1973) 5942-5946.

26. D.K. Lavallee, M.J. Bain-Ackerman, Bioinorg. Chem. 9 (1978) 311-321.

27. P.E.M. Siegbahn, M.R.A. Blomberg, Annu. Rev. Phys. Chem. 50 (1999) 221–249.

28. P.E.M. Siegbahn, M.R.A. Blomberg, Chem. Rev. 100 (2000) 421–437.

29. C. Rovira, K. Kunc, J. Hutter, P. Ballone, M. Parrinello, J. Phys. Chem. A 101 (1997) 8914-8925.

30. T.G. Spiro, P.M. Kozlowski, Acc. Chem. Res. 34 (2001) 137-144.

31. E. Sigfridsson, U. Ryde, J. Inorg. Biochem. 91 (2002) 116-124.

32. T. Andruniow, M.Z. Zgierski, P.M. Kozlowski, J. Phys. Chem. B, 104 (2000) 10921.

33. N. Dölker, F. Maseras, A. Lledos, J. Phys. Chem. B, 105 (2001) 7564.

34. K.P. Jensen & U. Ryde J. Mol. Struct. 585 (2002) 239-255.

35. A. Ghosh, T. Wondimagegn & H. Ryeng, Curr. Opin. Chem. Biol. 5 (2001) 744-750.

36. E. Sigfridsson & U. Ryde, J. Biol. Inorg. Chem. 8 (2002) 273-282.

37. A.D. Becke, Phys. Rev. A, 38 (1988) 3098.

38. J. P. Perdew, Phys. Rev. B, 33 (1986) 8822.

39. A. Schäfer, C. Huber & R. Ahlrichs, J. Chem. Phys. 100 (1994) 5829.

40. A. Schäfer, H. Horn, R. Ahlrichs, J. Chem. Phys. 97 (1992) 2571.

41. K. Eichkorn, Treutler, O.H. Öhm, M. Häser, Ahlrichs, R. Chem. Phys. Lett. 240 (1995) 283-290.
42. K. Eichkorn, F. Weigend, O. Treutler, R. Ahlrichs, Theor. Chem. Acc. 97 (1997) 119.
43. R.H. Hertwig, W. Koch, Chem. Phys. Lett. 268 (1997) 345.
44. P.E.M. Siegbahn, J. Comput. Chem. 22 (2001) 1634-1645.
45. A. Klamt, G. Schüürmann, J. Chem. Soc. Perkin Trans. 2 (1993) 799.
46. A. Schäfer, A. Klamt, D. Sattel, J.C.W. Lohrenz, F. Eckert, Phys. Chem. Chem. Phys 2 (2000) 2187-2193.
47. A. Klamt, V. Jonas, T. Bürger, J.C.W. Lohrenz, J. Phys. Chem. 102 (1998) 5074-5085.
48. F. Jensen, Introduction to Computational Chemistry 1999, John Wiley & Sons.
49. M.J. Frisch, G.W. Trucks, H.B. Schlegel, G.E. Scuseria, M.A. Robb, J.R. Cheeseman, V.G. Zakrzewski, J.A. Montgomery, R.E. Stratmann, J.C. Burant, S. Dapprich, J.M. Millam, A.D. Daniels, K.N. Knudin, M.C. Strain, O. Farkas, J. Tomasi, V. Barone, M. Cossi, R. Cammi, B. Mennucci, C. Pomelli, C. Adamo, S. Clifford, J. Ochterski,G.A. Petersson, P.Y. Ayala, Q. Cui, K. Morokuma, D.K. Malick, A.D. Rabuck, K. Raghavachari, J.B. Foresman, J. Cioslowski, J.V. Ortiz, B.B. Stefanov, G. Liu, A. Liashenko, P. Piskorz, I. Komaromi, R. Gomperts, R.L. Martin, D.J. Fox, T. Keith, M.A. Al-Laham, C.Y. Peng, A. Nanayakkara, C. Gonzalez, M. Challacombe, P.M.W. Gill, B.G. Johnson, W. Chen, M.W. Wong, J.L. Andres, M. Head-Gordon, E.S. Replogle, J.A. Pople 1998. Gaussian 98, Revision A.9, Gaussian, Inc. Pittsburgh PA.
50. K. Wolinski, J.F. Hinton, R. Pulay, J. Am. Chem. Soc. 112 (1990) 8251.
51. R. Ahlrichs, M. Bär, M. Häser, H. Horn, C. Kölmel, Chem. Phys. Lett. 162 (1989) 165.
52. U. Ryde & K. Nilsson, J. Am. Chem. Soc. ASAP article (2003)DOI: 10.1021/ja0365328
53. C.W. Bauschlicher, Chem. Phys. Lett. 246 (1995) 40.
54. U. Ryde, M.H.M. Olsson, Intern. J. Quant. Chem. 81 (2001) 335-347.
55. J.R. Hall, N.K. Marchant, R.A. Plowman, Aust. J. Chem. 15 (1962) 480.
56. M.P. Bryn, C.J. Curtis, Y. Hsiou, S.I. Khan, P.A. Sawin, S.K. Tendick, A. Terzis, C.E.

Strouse, J. Am. Chem. Soc. 115 (1993) 9480.

57. M.P. Bryn, C.J. Curtis, I. Goldberg, Y. Hsiou, S.I. Khan, P.A. Sawin, S.K. Tendick, C.E. Strouse, J. Am. Chem. Soc. 113 (1991) 6549.
58. B.S. Erler, W.F. Scholz, Y.J. Lee, W.R. Scheidt, C.A. Reed, J. Am. Chem. Soc. 109 (1987) 2644.
59. I. Csöregh, P. Kierkegaard, R. Norrestam, Acta Crystallogr. B 1975, 31, 314.
60. J.J.R. Fraústo da Silva, R.P.J. Williams The biological chemistry of the elements, Clarendon Press, Oxford, 1994.
61. A. Pasquarello, I. Petri, P.S. Salmon, O. Parisel, R. Car, É. Tóth, D.H. Powell, H.E. Fischer, L. Helm, A.E. Mebach, Science 291 (2001) 856-859.
62. M. Inamo, Kohagura, T. Kaljurand, I. Leito, I. Inorg. Chim. Acta, 340 (2002) 87-96.
63. T. Helgaker, M. Jaszunski, K. Ruud, Chem. Rev. 99 (1999) 293-352.
64. S.J. Baum, R.A. Plane, J. Am. Chem. Soc. 88 (1966) 910-913.
65. M.J. Bain-Ackerman, D.K. Lavallee, Inorg. Chem. 18 (1979) 3358-3364.

Table 1. Metal–ligand distances (pm) in the optimised SAT structures with Mg^{2}+ and only first-sphere water molecules (complexes with also second-sphere can be found in Table S1 in the supplementary material). If not otherwise stated (cis and 1N), it is assumed that they have the hydrogens of $PorH_2$ in trans positions and that the metal ion binds two N_{Pyrn} atoms.

Complex	Metal–ligand distance (pm)		
	N_{Pyrn}	N_{Pyrn}	O
1+0	212.6, 212.7	226.0, 226.2	205.0
1+0 cis	208.0, 208.4	231.7, 232.2	205.9
2+0	221.9, 221.9	236.7, 237.8	211.7, 212.9
2+0 1N	206.6, 342.4	224.2, 336.3	192.1, 203.0
2+0 cis	211.4, 211.7	254.4, 254.8	206.9, 218.4
3+0	232.1, 233.0	230.8, 281.3	212.7, 215.7, 219.0
3+0 1N	210.3, 361.3	249.8, 338.4	197.4, 204.8, 208.7
3+0 cis	211.9, 217.4	329.5, 340.3	207.2, 207.5, 212.0
4+0	243.5, 246.7	266.6, 267.4	222.7, 223.4, 223.7, 223.7
4+0 1N	214.2, 409.9	339.3, 341.2	202.9, 206.4, 206.8, 214.3
4+0 cis	222.2, 222.8	361.0, 361.7	209.1, 215.2, 218.1, 222.2
5+0 1N	230.5, 429.4	360.3, 368.2	205.8, 211.3, 211.9, 213.1, 214.5
5+0 cis 1N	229.5, 437.7	361.3, 367.5	205.0, 210.5, 210.7, 214.7, 215.8
6+0	414.5, 449.2	390.1, 507.9	204.1, 210.4, 210.8, 211.1, 211.2, 213.4
MgPor	207.3*4	-	-
$Mg(H_2O)_6$	-	-	209.8,209.9*3,210.1*2

Table 2. Relative energy of the various SAT complexes with Mg^{2+} (named in the same way as in Table 1). Values in brackets are relative free energies (ΔG), including zero-point and thermal effects.

Complex	Relative Energy (kJ/mole)		$PorH_2$ distortion
	Vacuum	Water	energy (kJ/mole)
1+0	0.0	0.0	195.4
1+0 cis	15.0	6.1	222.8
2+0	0.0	0.0	158.1
2+0 1N	41.6	40.3	95.3
2+0 cis	7.2	0.2	182.9
1+1	-19.3	0.9 (2.1)	182.7
3+0	0.0	0.0	120.1
3+0 1N	-7.5	-8.1 (-16.4)	75.5
3+0 cis	-15.4	-14.8	111.9
2+1	-18.9	-4.2 (-5.8)	-
1+2	-31.4	1.7	-
4+0	0.0	0.0	92.8
4+0 1N	-71.4	-82.6 (-88.9)	39.3
4+0 cis	-43.9	-45.2	105.2
3+1	-49.7	-42.6 (-51.5)	-
3+1 1N	-87.1	-78.2 (-94.1)	-
3+1 cis	-49.7	-38.0	-
2+2	-77.9	-61.5	140.7
1+3	-66.2	-43.6	-
5+0 1N	0.0	0.0	35.7
5+0 1N cis	40.6	32.8	81.2
4+1	80.1	88.7 (92.7)	-
4+1 1N	-24.4	-20.1 (-14.6)	36.3
4+1 cis	10.2	21.5	-
6+0	0.0	0.0	27.5
5+1 1N	-11.6	10.7 (21.0)	34.5
4+2	99.0	123.8	-
4+2 1N	-28.5	-1.1	33.7
4+2 cis	10.4	39.8	-
3+3	28.9	58.6	-

3+3 1N	-7.5	32.3	-
3+3 cis	28.9	59.9	-
2+4	11.9	61.7	145.6
1+5	31.9	60.4	167.4

Table 3. Metal–ligand distances (pm) and copper spin population in the optimised SAT structures with Cu^{2}+ and water (named in the same way as in Table 1).

Complex	Metal–ligand distance (pm)			Cu
	N_{Pyrn}	N_{Pyrn}	O / N_{An}	Spin
1+0	201.7, 201.7	218.5, 218.5	221.5	0.46
1+0 cis	198.7, 198.7	221.1, 222.2	222.0	0.51
2+0	225.5, 225.5	247.3, 260.7	208.5, 208.6	0.44
2+0 1N	190.4, 365.0	300.5, 310.9	198.3, 203.8	0.26
2+0 Cu^{I}	209.7, 209.8	265.1, 265.1	218.4, 218.5	0.29
2+0 cis	198.1, 199.1	308.8, 310.3	202.8, 206.0	0.51
2+0 altcis	195.4, 315.1	224.4, 299.4	196.0, 214.6	0.39
3+0 1N	205.2, 418.9	339.2, 353.6	199.9, 206.2, 214.6	0.39
3+0 1N Cu^{I}	191.1, 372.1	309.0, 313.2	200.7, 209.4, 231.5	0.32
4+0 1N	205.6, 420.0	343.5, 349.2	201.9, 203.7, 222.6, 229.7	0.44
2(Cu 3+0)	209.3, 538.3	400.6, 409.4	201.5, 205.9, 209.3	0.41
	211.6, 542.6	397.5, 413.0	199.1, 204.2, 215.2,	0.42
2(Cu 3+0) Cu^{I}	208.7, 546.2	405.2, 410.7	203.3, 206.8, 212.9	0.37
	206.7, 540.4	395.8, 412.1	203.6, 207.5, 212.3	0.33
CuPor	202.4*4	-	-	0.50
$Cu(H_2O)_6$	-	-	196.0, 196.1, 198.7, 199.4, 360, 377	0.59
$Cu(H_2O)_4$	-	-	196.2, 196.9, 200.3, 200.3	0.62

Table 4. Relative energy of the various SAT complexes with Cu^{2+} and water (named in the same way as in Table 1).

Complex	Relative Energy (kJ/mole)		$PorH_2$ distortion
	Vacuum	Water	energy (kJ/mole)
1+0	0.0	0.0	212.5
1+0 cis	18.4	9.6	241.0
2+0	73.8	74.7	98.9
2+0 Cu^{I}	57.1	65.2	98.9
2+0 1N	8.4	29.1	47.4
2+0 cis	0.0	0.0	123.3
2+0 altcis	28.0	41.9	88.7
1+1	-12.2	10.5	204.2
3+0 1N	35.0	28.8	31.0
3+0 1N Cu^{I}	30.8	34.7	44.5
2+1 1N	2.1	3.9	-
2+1 cis	0.0	0.0	118.3
2+1 altcis	40.9	41.3	83.1
1+2	16.1	25.5	-
4+0 1N	47.8	29.5	32.8
3+1 1N	11.9	9.4	31.7
2+2 Cu^{I}	52.7	63.4	-
2+2 1N	3.5	4.5	-
2+2 cis	0.0	0.0	110.2
2+2 altcis	23.2	25.3	89.3
1+3	30.8	37.3	-
4+1 1N	0.0	0.0	31.1
2(Cu 3+0)	0.0	0.0	64.6
2(Cu 3+0) Cu^{I}	12.1	-22.78	81.0

Table 5. Metal–ligand distances (pm) in the optimised sitting-atom structures with Cu^{2}+ and AN (named in the same way as in Table 1). The word "constr" means that the structure has been constrained and the constraints are marked in bold face in the table, whereas "solv" means that the structure has been optimised in a solvent with a dielectric constant of 36.64.

Complex	Metal–ligand distance (pm)			Cu
	N_{Pyrn}	N_{Pyrn}	N_{An}	Spin
1+0	204.4, 204.4	220.1, 220.2	209.9	0.46
1+0 solv	204.0, 204.0	218.8, 218.8	209.4	0.46
1+0 constr	205, 205	232, 232	198, 198	0.42
2+0 constr	205, 205	256.9, 257.0	198, 198	0.53
2+0 Cu^{I}	224.5, 224.6	283.4, 283.4	198.2, 198.2	0.20
2+0 Cu^{I} constr	205, 205	277.7, 277.8	198, 198	0.28
2+0 cis	201.4, 203.5	319.6, 328.2	198.8, 199.6	0.48
2+0 cis, solv	201.8, 201.8	311.4, 312.5	197.8, 197.9	0.50
2+0 cis, constr	205, 205	320.8, 328.6	198, 198	0.49
2+0 1N	197.4, 430.9	346.5, 346.8	190.9, 196.0	0.16
2+0 1N constr	205, 440.5	354.3, 354.8	198, 198	0.16
3+0 1N	208.3, 447.2	360.6, 365.7	198.1, 199.5, 200.2	0.20
3+0 1N, solv	206.9, 430.5	349.0, 353.6	197.5, 197.9, 199.0	0.23
3+0 1N, constr	205, 446.8	360.0, 363.2	198, 198, 198	0.21
3+0 cis	206.8, 207.2	333.3, 334.6	202.1, 202.3, 223.2	0.51
3+0 cis constr	205, 205	332.2, 334.0	198, 198, 232	0.55
3+0 trans constr	205, 205	263.5, 301.9	198, 198, 232	0.54
4+0 constr	205, 205	309.2, 310.2	198, 198, 232, 232	0.56
4+0 cis constr	205, 205	367.2, 368.2	198, 198, 232, 232	0.55
4+0 1N constr	205, 456.9	366.7, 366.7	198, 198, 232, 232	0.31
5+0 1N constr	205, 489.1	391.7, 392.8	198, 198, 198, 232, 232,	0.50
2(Cu2+0) 1N	199.5, 512.2	381.9, 389.8	191.5, 195.3	0.34
	203.1, 536.1	385.9, 416.9	191.7, 195.1	0.31
2(Cu2+0) altcis constr	205, 205	364.4, 365.1	198, 198	0.48
	205, 205	363.7, 364.8	198, 198	0.48
2(Cu3+0) 1N	214.5, 532.4	395.4, 412.3	198.1, 199.0, 200.7	0.36
	214.2, 532.4	394.4, 413.2	198.1, 199.1, 200.7	0.36

2(Cu3+0) 1N constr	205, 526.3	388.0, 404.8	198, 198, 198	0.35
	205, 525.7	387.9, 404.4	198, 198, 198	0.35
2(Cu4+0) altcis constr	205, 205	391.6, 406.4	198, 198, 232, 232	0.54
	205, 205	391.9, 406.2	198, 198, 232, 232	0.54
2(Cu 5+0) 1N constr	205, 544.5	400.3, 401.7	198, 198, 198, 198, 198	0.55
	205, 529.9	394.2, 395.2	198, 198, 198, 198, 198	0.55
CuPor	202.4*4	-	-	0.50
$CuAn_5$ trig. bipyramid	-	-	197.2, 197.2, 204.1, 204.1, 204.2	0.64
$CuAn_5$ square pyramid	-	-	198.8, 198.8, 199.0, 199.0, 214.1	0.64
$CuAn_6$	-	-	199.8*4, 238.3, 238.8	0.66

Table 6. Relative energy of the various SAT complexes with Cu^{2}+ and acetonitrile (named in the same way as in Table 1). The word "constr" means that the structure has been constrained to the distances observed in EXAFS (cf. Table 5).

Complex	Relative Energy (kJ/mole)		$PorH_2$ distortion
	Vacuum	Acetonitrile	energy (kJ/mole)
1+0	0.0	0.0	198.9
1+0 constr	7.0	9.9	-
2+0 constr	95.6	82.0	162.5
2+0 Cu^{I}	40.7	45.1	64.4
2+0 Cu^{I} constr	52.5	53.0	-
2+0 1N	-5.1	13.8	27.2
2+0 1N constr	-0.5	19.0	-
2+0 cis	0.0	0.0	112.0
2+0 cis constr	0.4	0.6	-
1+1	44.8	37.8	-
3+0 1N	0.0	0.0	25.1
3+0 1N constr	0.4	0.1	-
3+0 cis	18.2	-6.6	101.2
3+0 cis constr	19.9	-5.4	-
2+1 1N	28.0	35.3	-
2+1 cis	22.2	21.8	-
1+2	85.0	59.9	-
4+0 constr	217.4	188.5	168.1
4+0 cis constr	82.9	74.2	132.4
4+0 1N constr	44.6	32.3	28.7
3+1 1N	0.0	0.0	-
3+1 cis	26.9	21.9	-
2+2 cis	23.3	32.9	-
1+3	100.1	61.0	-
5+0 1N constr	77.7	42.3	53.6
3+2 1N	0.0	0.0	-
2(Cu 2+0) 1N	0.0	0.0	68.8
2(Cu 2+0) altcis constr	107.1	45.7	154.9
2(Cu 3+0) 1N	0.0	0.0	54.2
2(Cu 3+0) constr	4.0	1.8	62.7

2(Cu 3+1) 1N	0.0	0.0	-
2(Cu 4+0) altcis constr	236.0	145.5	200.9
2(Cu 3+2) 1N	0.0	0.0	-
2(Cu 5+0) 1N constr	96.43	34.27	115.8

Table 7. Hydrogen NMR shifts relative free porphyrin ($PorH_2$ in the calculations and free tetraphenylporphyrin in the experiment [22]) for the pyrrole NH group and the β pyrrole hydrogen atoms with various interactions of the pyrrole nitrogen atoms (NH, N–Cu, or with no interaction). Values for each individual hydrogen atom is given for the calculations.

Complex	Chemical shift relative to $PorH_2$ (ppm)			
	H–N	H [?]; N_{Pyr}–H	H [?]; N_{Pyrn}–Cu	H [?]; N_{Pyrn}
2+0 trans	+1.58,+1.59	–1.22,–1.22,–1.23,–1.24	–1.06,–1.07,–1.08,–1.09	–
3+0 trans constr	+0.32,+1.51	–0.95,–0.96,–1.21,–1.21	–1.06,–1.07,–1.15,–1.15	–
4+0 constr	–0.72,–0.74	–0.79,–0.79,–0.79,–0.80	–0.90,–0.91,–0.91,–0.92	–
3+0 1N	–31.37,–31.64	+3.67,+3.69,+3.81,+3.89	+2.87,+2.97	+3.01,+3.01
3+0 1N Zn	+0.80,+0.89	–0.75,–0.82,–0.95,–0.98	–0.61,–0.69	–0.61,–0.69
4+0 1N	–23.26,–23.31	+2.37,+2.37,+2.68,+2.69	+1.89,+1.90	+1.94,+1.94
4+0 1N Zn	+0.68,+0.69	–0.65,–0.66,–0.90,–0.91	–0.47,–0.48	–0.44,–0.44
5+0 1N constr	–0.93,–1.07	–0.21,–0.22,–0.66,–0.69	–0.13,–0.24	–0.33,–0.34
2+0 cis	+1.82,+2.70	–1.10,–1.15,–1.34,–1.49	–0.91,–1.03,–1.05,–1.12	–
3+0 cis	+1.19,+1.74	–0.96,–0.98,–1.29,–1.31	–0.59,–0.65,–0.94,–0.98	–
4+0cis constr	+0.37,+1.98	–0.69,–0.77,–0.84,–1.03	–0.11,–0.12,–0.71,–0.71	–
CuPor	–	–	–0.77,–0.77,–0.77,–0.77 –0.78,–0.78,–0.78,–0.78	–
$PorH_4^{2+}$	+3.43.+3.43 +3.44,+3.46	–1.45,–1.45,–1.45,–1.45 –1.46,–1.46,–1.46,–1.46	–	–
experiment	+0.82	–0.19	–0.08	–

Table 8. Metal–ligand distances (pm) in the optimised sitting-atom structures with Fe^{2}+ and water (named in the same way as in Table 1).

Complex	Metal–ligand distance (pm)			Fe
	N_{Pyrn}	N_{Pyrn}	O / N_{An}	spin
1+0	207.5, 207.5	227.5, 228.3	207.2	3.64
1+0 cis	202.3, 203.4	235.1, 236.0	208.6	3.64
2+0	214.1, 214.2	239.6, 239.6	217.4, 217.4	3.65
2+0 cis	200.2, 204.3	295.1, 300.0	207.2, 214.2	3.69
3+0	221.1, 223.6	238.6, 256.0	223.2, 225.2, 231.8	3.68
3+0 cis	205.7, 209.0	318.4, 318.8	214.9, 218.1, 221.3	3.68
3+0 1N	206.0, 405.9	331.0, 334.1	185.2, 212.4, 213.7	3.66
4+0	237.1, 238.0	258.8, 260.0	228.8, 229.1, 229.4, 229.8	3.70
4+0 cis	214.3, 214.6	358.7, 358.8	210.6, 215.7, 229.5, 236.3	3.72
4+0 1N	214.7, 428.9	349.8, 352.9	187.7, 220.5, 220.6, 225.5	3.70
5+0 1N	225.5, 451.5	364.3, 367.3	192.9, 217.5, 220.3, 226.5, 227.9	3.74
6+0	408.9, 458.2	427.8, 429.3	204.4, 204.7, 218.6, 219.0, 219.8, 229.8	3.75
2(Fe 4+0) 1N	208.0, 545.1	404.7, 408.0	209.2, 213.9, 221.9, 221.9	3.72
	209.2, 547.2	404.5, 412.5	209.8, 210.6, 215.5, 226.7	3.72
FePor	206.1*4	-	-	3.69
FePor$(H_2O)_2$	207.6*4	-	232.7, 232.9	3.82
$Fe(H_2O)_6$	-	-	(212.2,214.7,217.6)*2	3.78

Table 9. Relative energy of the various SAT complexes with Fe^{2+} (named in the same way as in Table 1). Values in brackets are relative free energies (ΔG), including zero-point and thermal effects.

Complex	Relative Energy (kJ/mole)		$PorH_2$ distortion
	Vacuum	Water	energy (kJ/mole)
1+0	0.0	0.0	191.4
1+0 cis	12.2	6.6	216.9
2+0	0.0	0.0	167.2
2+0 cis	3.5	-1.1	134.0
1+1	-35.4	-16.9	-
3+0	0.0	0.0	134.5
3+0 1N	-42.7	-34.6 (-43.1)	59.0
3+0 cis	-13.8	-17.9	112.0
2+1	-24.0	-16.0 (-28.9)	-
2+1 cis	-40.7	-33.2	-
1+2	-49.7	-25.0	-
4+0	0.0	0.0	91.5
4+0 1N	-69.0	-56.3	45.4
4+0 cis	-23.6	-23.2	111.1
3+1	-29.0	-22.0 (-48.0)	-
3+1 1N	-102.4	-78.8	-
2+2	-69.7	-57.8	-
2+2 cis	-81.3	-61.8	-
1+3	-93.1	-70.3	-
5+0 1N	0.0	0.0	68.7
4+1	67.4	69.5 (70.6)	-
4+1 1N	-32.2	-24.7 (-5.2)	-
6+0	81.9	46.4	31.1
5+1 1N	22.1	20.6 (9.5)	-
4+2	107.1	99.8	-
4+2 1N	0.0	0.0	-
4+2 cis	69.1	66.6	-
3+3	46.4	45.5	-
3+3 cis	48.6	48.3	-

2+4	14.2	29.5	-
2+4 cis	4.7	19.2	-
1+5	57.8	69.8	-
1+5 cis	72.4	76.4	-
2Fe 4+0	0.0	0.0	90.1

Table 10. Metal-ion binding energies (kJ/mole) in vacuum and solution for the various complexes (named in the same way as in Table 1).

Complex	Mg^{2+} complexes		Fe^{2+} complexes		Cu^{2+}– water complexes		Cu^{2+}– AN complexes	
	ε = 1	ε = 80	ε = 1	ε = 80	ε = 1	ε = 80	ε = 1	ε = 36.64
1+0	1211.5	390.1	1435.8	610.7	1684.1	851.6	1710.9	838.5
1+0 cis	1196.4	384.0	1423.6	604.1	1665.7	842.1		
2+0	1266.1	410.7	1503.3	645.9	1693.6	832.1	1764.3	831.5
2+0 1N	1224.5	370.4			1742.3	868.2	1810.1	862.8
2+0 cis	1258.9	410.6	1499.9	647.0	1750.7	897.3	1809.0	876.6
3+0	1312.3	423.6	1569.3	673.0				
3+0 1N	1319.8	431.7	1583.1	690.9	1819.1	908.3	1885.3	900.4
3+0 cis	1327.7	438.4	1612.0	707.6			1856.5	880.2
4+0	1319.7	390.9	1620.2	687.6				
4+0 1N	1391.1	473.5	1689.2	743.9	1888.3	959.3	1935.7[b]	914.8[b]
4+0 cis	1363.6	436.2	1643.8	710.8				
5+0 1N	1451.3	487.7	1766.9	789.3	1993.1[a]	1009.6[a]	1977.7[c]	905.3[c]
6+0	1509.1	522.4	1808.2	822.6				
$M(H_2O)_4$					1475.3	878.8	1731.2	862.9
$M(H_2O)_6$	1322.1	550.0	1556.4	789.6	1777.6	1016.7	1899.8	913.2
MPor	2866.9	828.8	3123.0	1058.7	3436.9	1377.9	3436.9	1377.9

[a] The 4+1 complex.

[b] The 3+1 1N complex.

[c] The 3+2 1N complex.

Legends to the figures

Figure 1. Optimised structures of sitting-atop complexes of Mg^{2+} with various numbers of water ligands: (a) 5+0 1N, (b) 5+0 1N cis, (c) 4+0, (d) 4+0 1N, (e) 4+0 cis, (f) 3+0, (g) 3+0 1N, (h) 3+0 cis, (i) 2+0, (j) 2+0 1N, (k) 2+0 cis, (l) 1+0, (m) 1+0 cis.

Figure 2. Optimised structures of sitting-atop complexes of Cu^{2+} with various numbers of water ligands: (a) 4+0, (b) 3+0 1N, (c) 3+0 Cu^{I} 1N, (d) 2+0, (e) 2+0 Cu^{I}, (f) 2+0 cis, (g) 2+0 altcis, (h) 2+0 1N, (i) 1+0, (j) 2(Cu 3+0) 1N, (k) 2(Cu 3+0) Cu^{I} 1N.

Figure 3. Optimised structures of sitting-atop complexes of Cu^{2+} with various numbers of acetonitrile ligands: (a) 4+0 constrained, (b) 4+0 1N, constrained, (c) 4+0 cis, constrained, (d) 3+0 cis, (e) 3+0 cis, constrained, (f) 3+0 1N, (g) 2+0 Cu^{I}, (h) 2+0 cis, (i) 2+0 1N, (j) 1+0, (k) 2(Cu 2+0) 1N, (l) 2(Cu 3+0) 1N, (m) 2 (Cu 2+0) altcis, constrained.

Figure 4. Optimised structures of sitting-atop complexes of Fe^{2+} with various numbers of water ligands: (a) 5+0 1N, (b) 4+0, (c) 4+0 1N, (d) 4+0 cis, (e) 3+0, (f) 3+0 1N, (g) 3+0 cis, (h) 2+0, (i) 2+0 cis, (j) 1+0, (k) 2(Fe 4+0) 1N.

Figure 5. Optimised structures of sitting-atop complexes of Fe^{2+} with PorHCH3 and two water ligands (cis and trans structure).

Figure 6. Optimised structures of $PorH_2$ hydrogen bonded to two or four water molecules, showing that the porphyrin may be expected to be non-planar also in water solution.

Figure 1. Optimised structures of sitting-atop complexes of Mg^{2+} with various numbers of water ligands: (a) 5+0 1N, (b) 5+0 1N cis, (c) 4+0, (d) 4+0 1N, (e) 4+0 cis, (f) 3+0, (g) 3+0 1N, (h) 3+0 cis, (i) 2+0, (j) 2+0 1N, (k) 2+0 cis, (l) 1+0, (m) 1+0 cis.

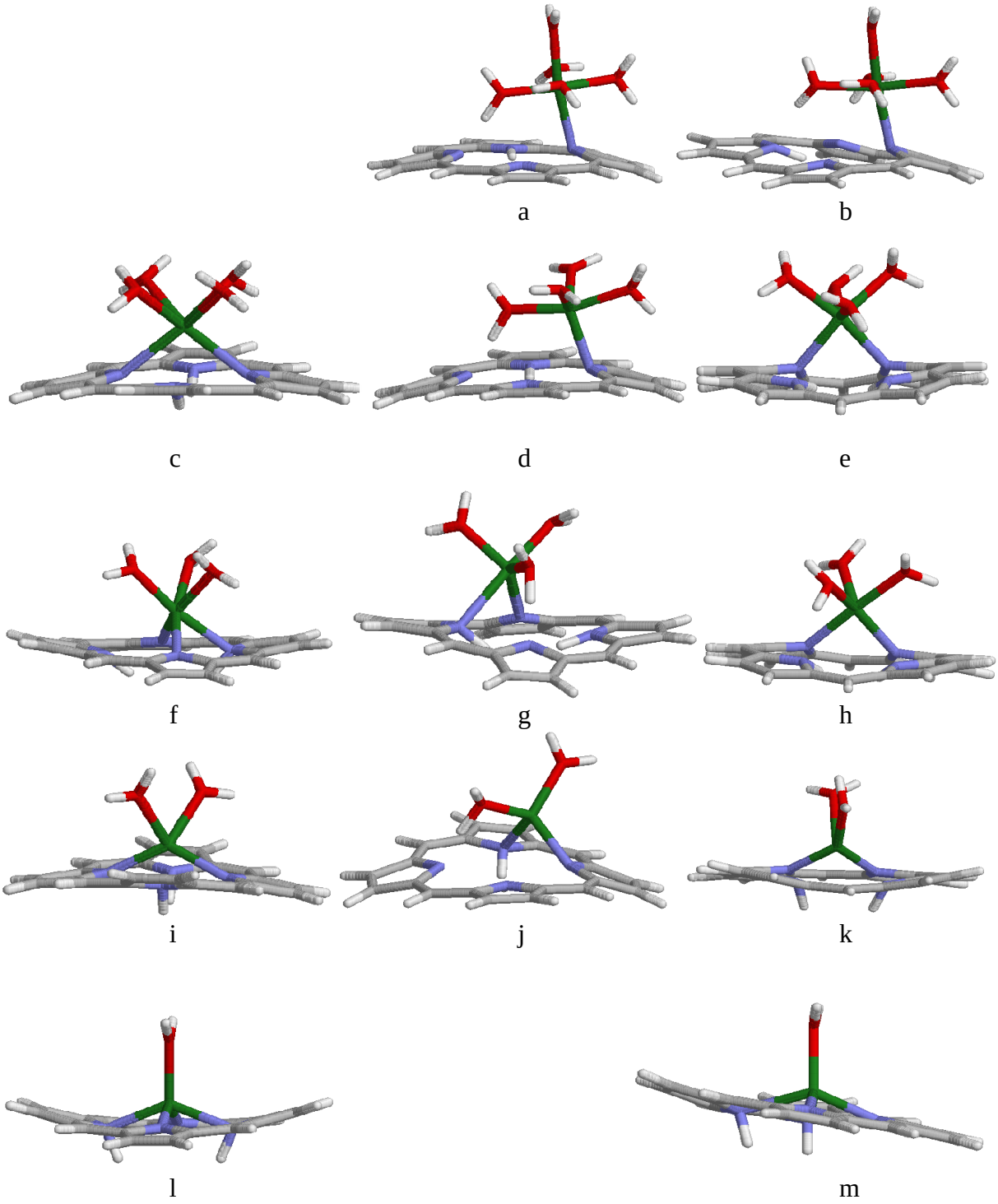

Figure 2. Optimised structures of sitting-atop complexes of Cu^{2+} with various numbers of water ligands: (a) 4+0, (b) 3+0 1N, (c) 3+0 Cu^{I} 1N, (d) 2+0, (e) 2+0 Cu^{I}, (f) 2+0 cis, (g) 2+0 altcis, (h) 2+0 1N, (i) 1+0, (j) 2(Cu 3+0) 1N, (k) 2(Cu 3+0) Cu^{I} 1N.

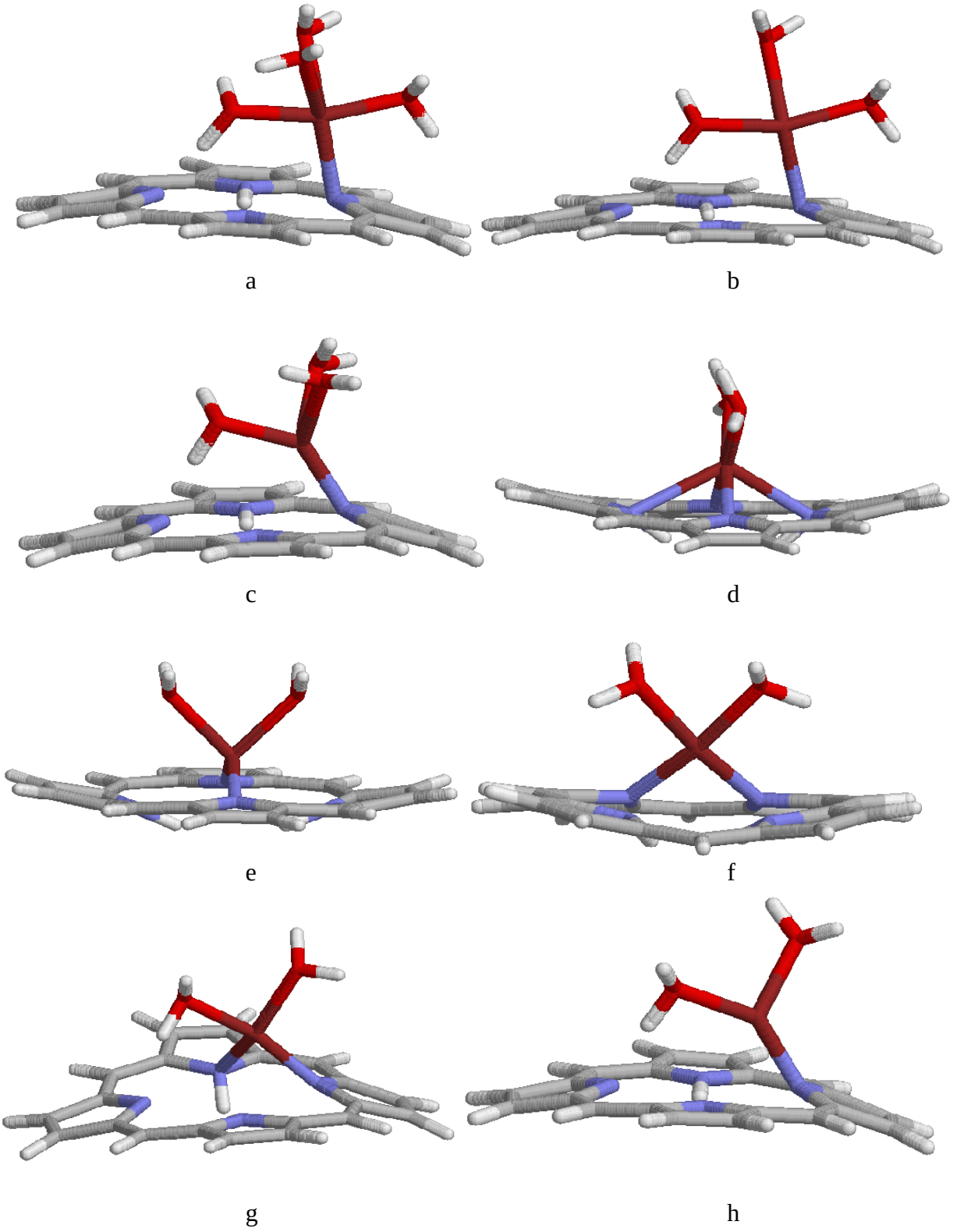

a b c d e f g h

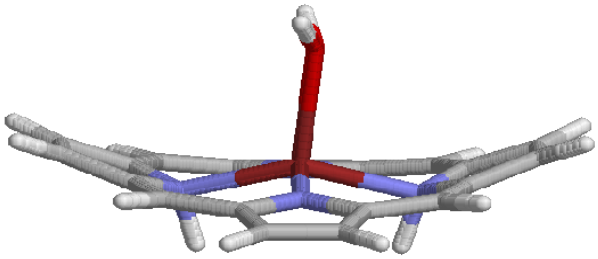

i

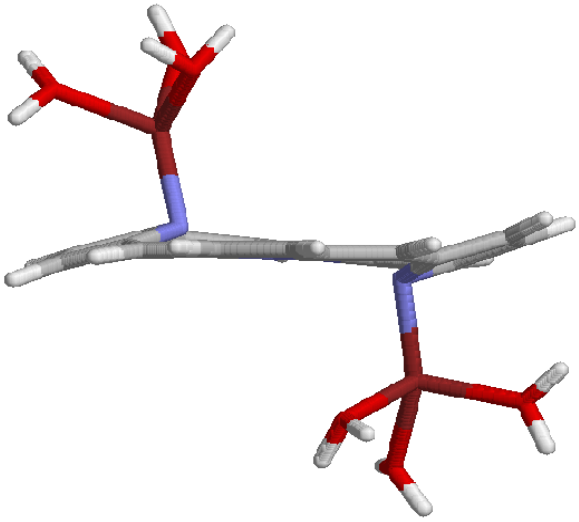

j

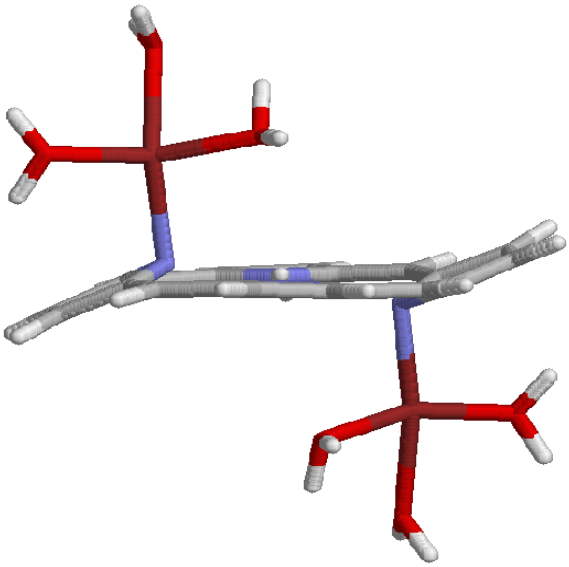

k

Figure 3. Optimised structures of sitting-atop complexes of Cu^{2+} with various numbers of acetonitrile ligands: (a) 4+0 constrained, (b) 4+0 1N, constrained, (c) 4+0 cis, constrained, (d) 3+0 cis, (e) 3+0 cis, constrained, (f) 3+0 1N, (g) 2+0 Cu^{I}, (h) 2+0 cis, (i) 2+0 1N, (j) 1+0, (k) 2(Cu 2+0) 1N, (l) 2(Cu 3+0) 1N, (m) 2 (Cu 2+0) altcis, constrained.

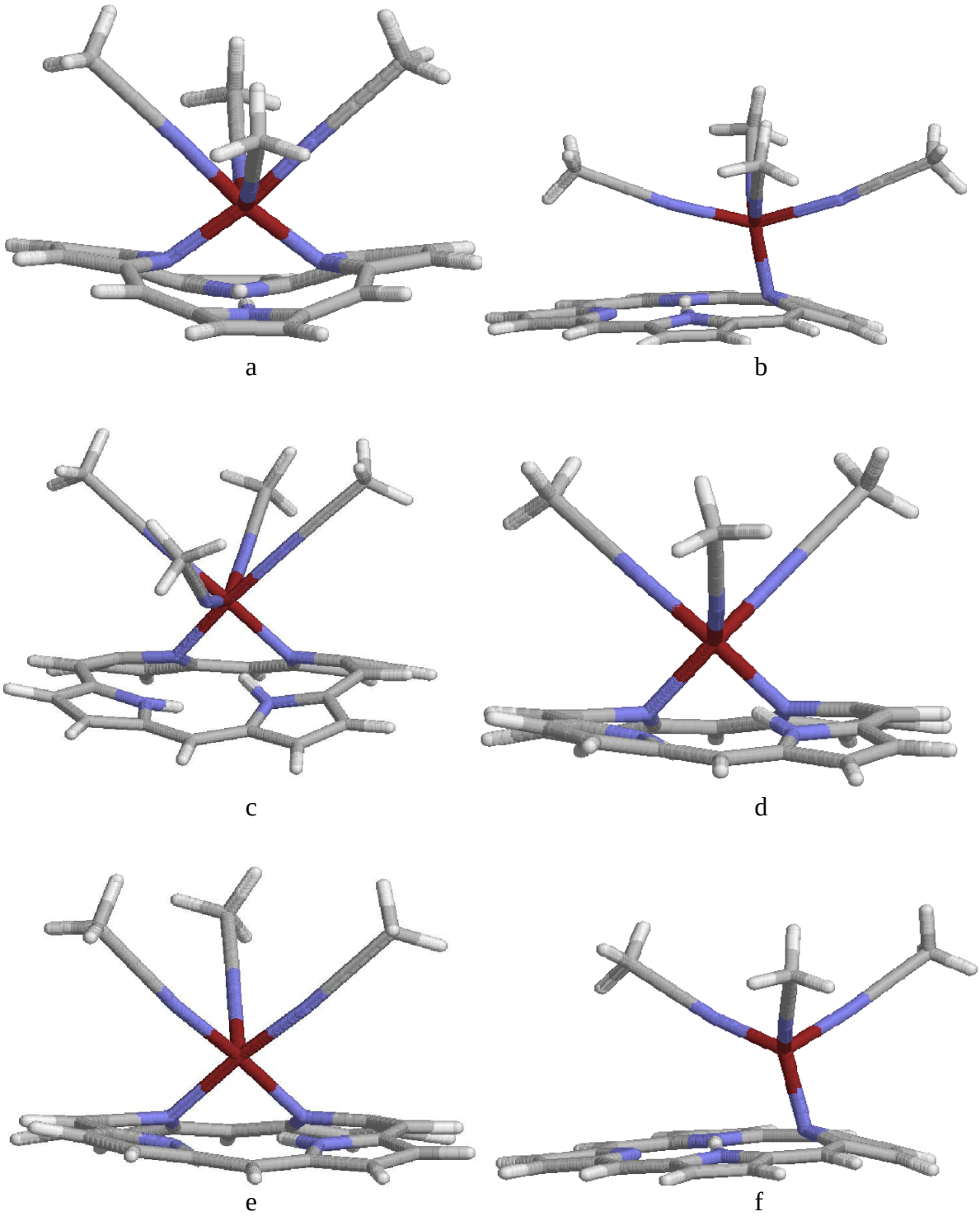

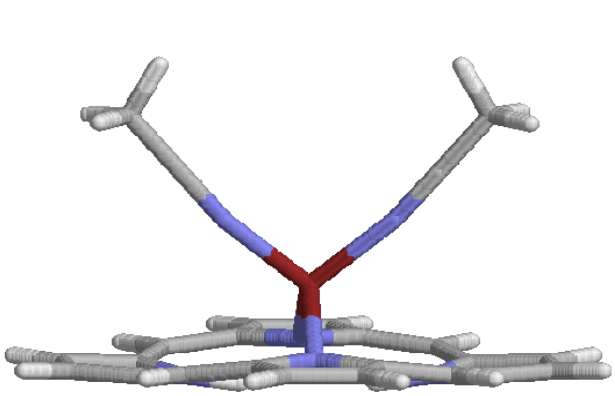

g

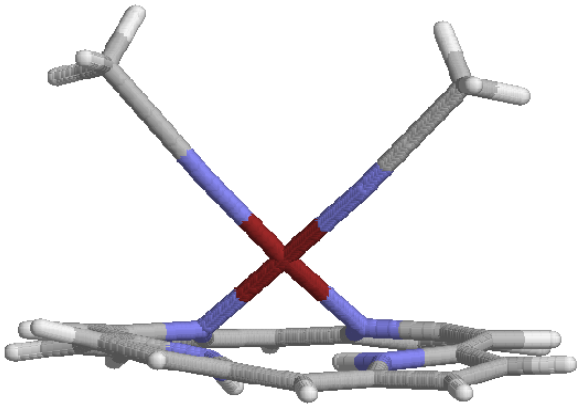

h

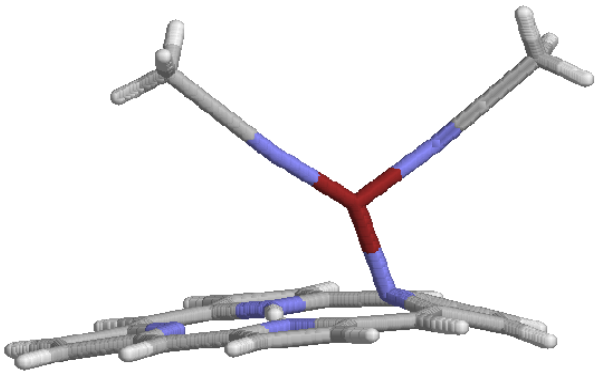

i

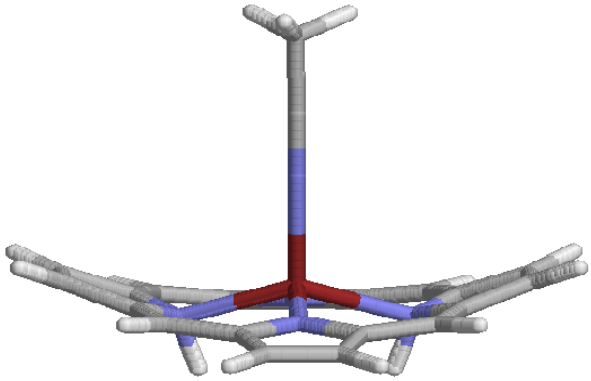

j

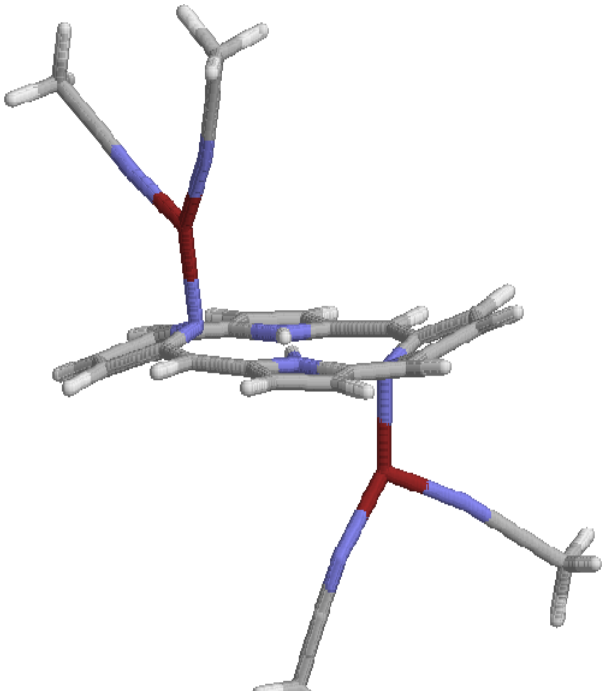

k

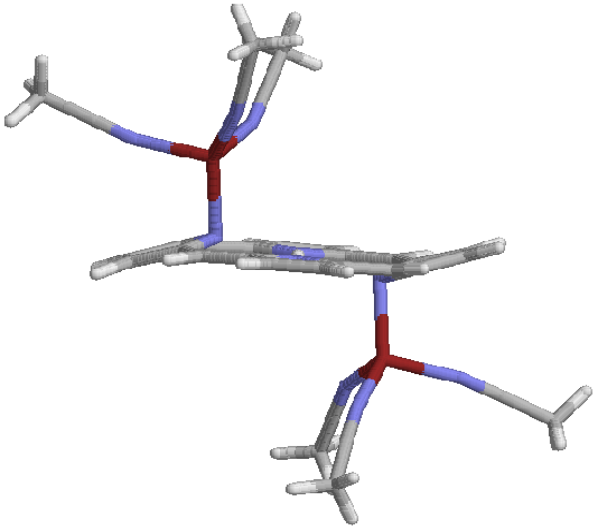

l

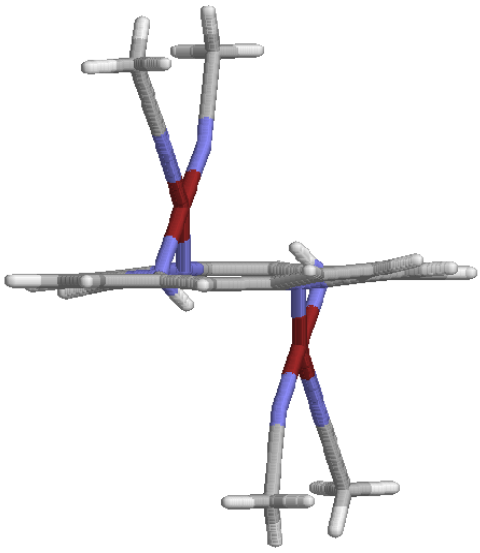

m

Figure 4. Optimised structures of sitting-atop complexes of Fe^{2+} with various numbers of water ligands: (a) 5+0 1N, (b) 4+0, (c) 4+0 1N, (d) 4+0 cis, (e) 3+0, (f) 3+0 1N, (g) 3+0 cis, (h) 2+0, (i) 2+0 cis, (j) 1+0, (k) 2(Fe 4+0) 1N.

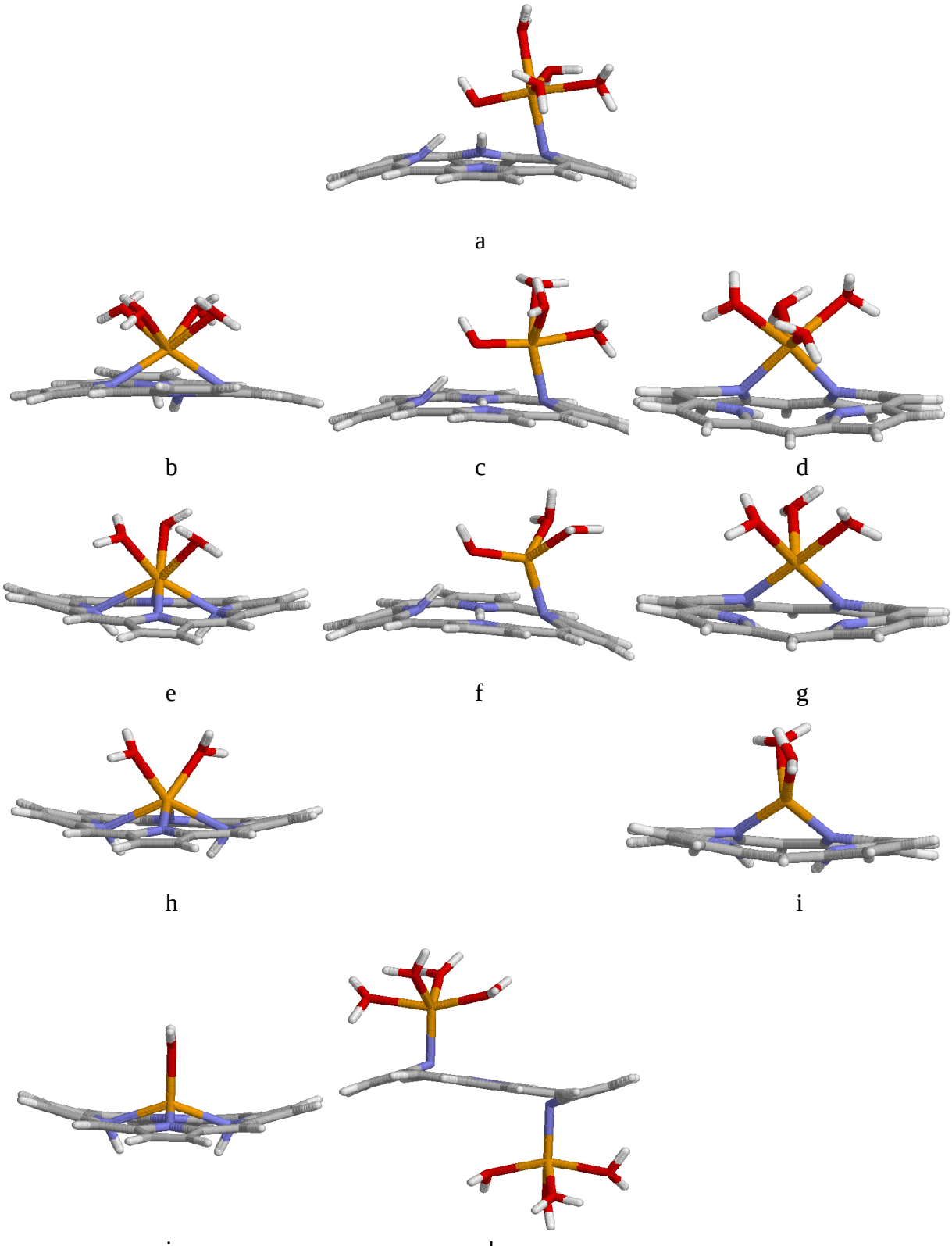

Figure 5. Optimised structures of sitting-atop complexes of Fe^{2+} with PorHCH3 and two water ligands (cis and trans structure).

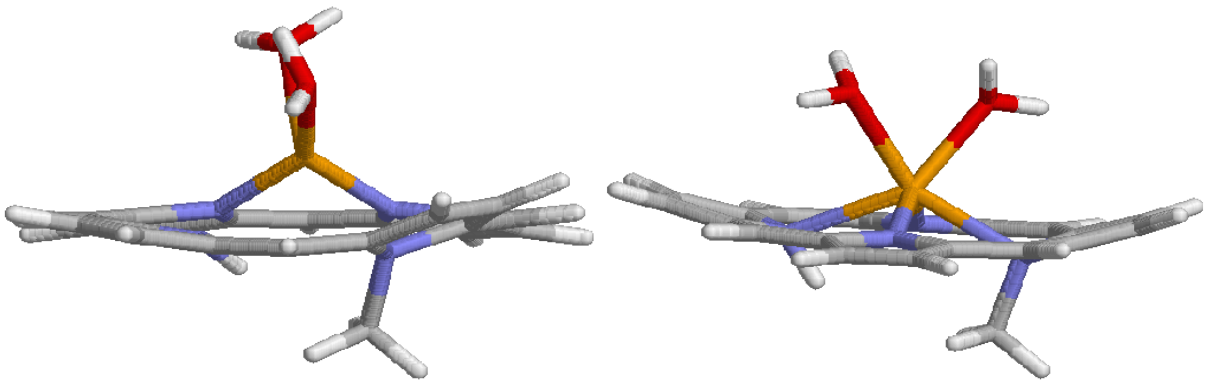

a b

Figure 6. Optimised structures of $PorH_2$ hydrogen bonded to two or four water molecules, showing that the porphyrin may be expected to be non-planar also in water solution.

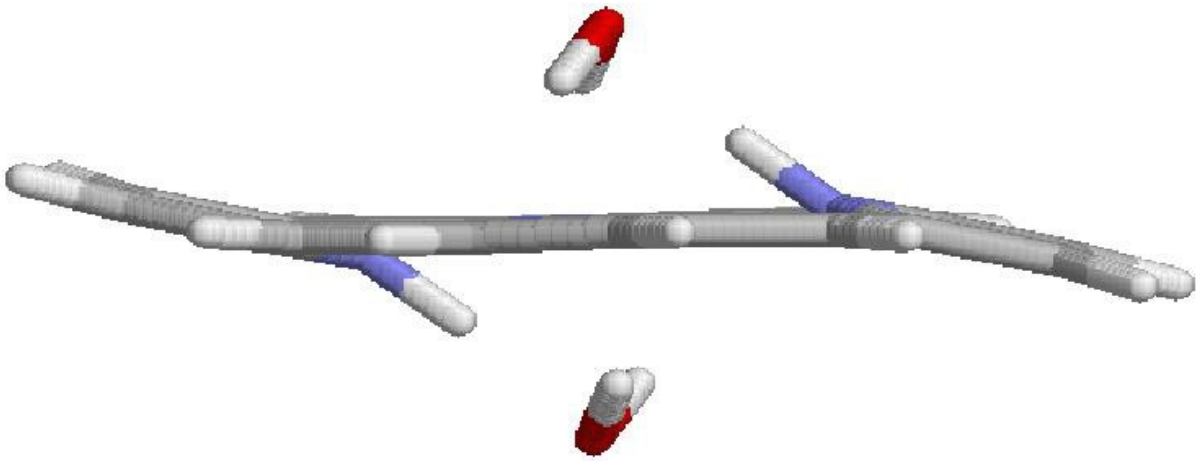

a

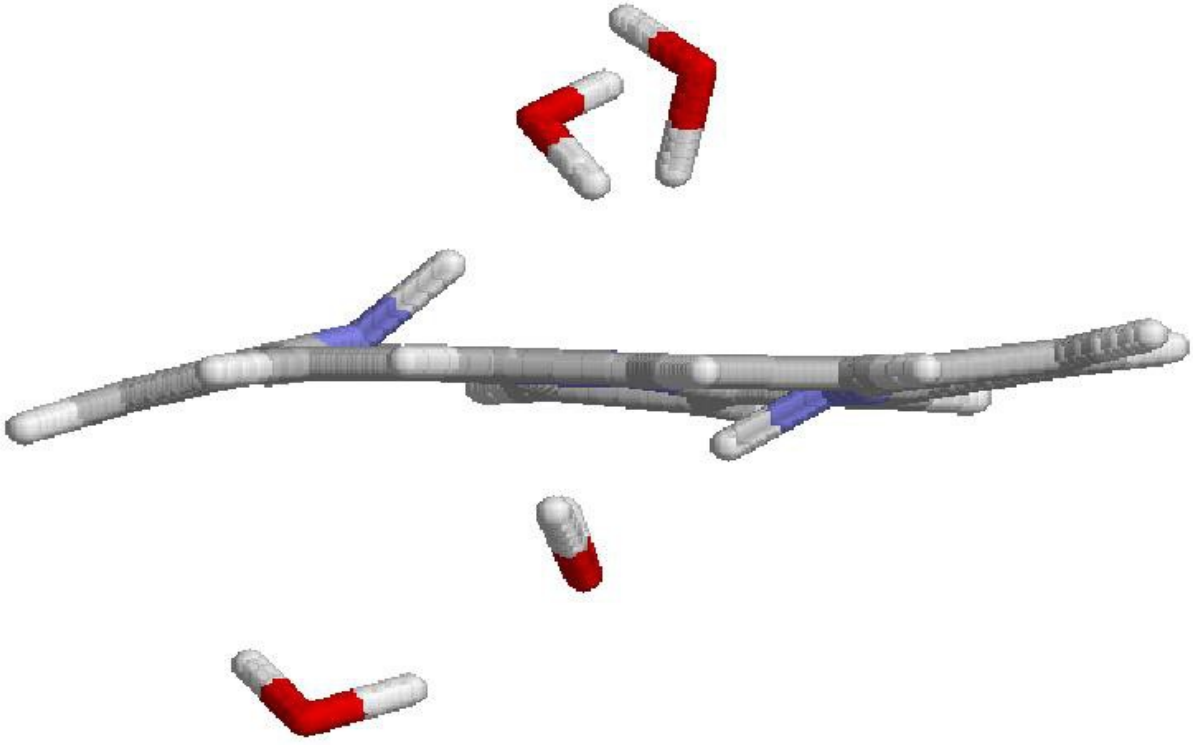

b